AD-A190 510 THE GROWTH OF CORNER CRACKS UNDER THE CONJOINT ACTION OF HIGH AND LOW CYCLE FATIGUE(U) B E POWELL ET AL. 1/1
FEB 88 AFWAL-TR-87-4130 F49620-85-C-0116

UNCLASSIFIED F/G 11/6.1 NL

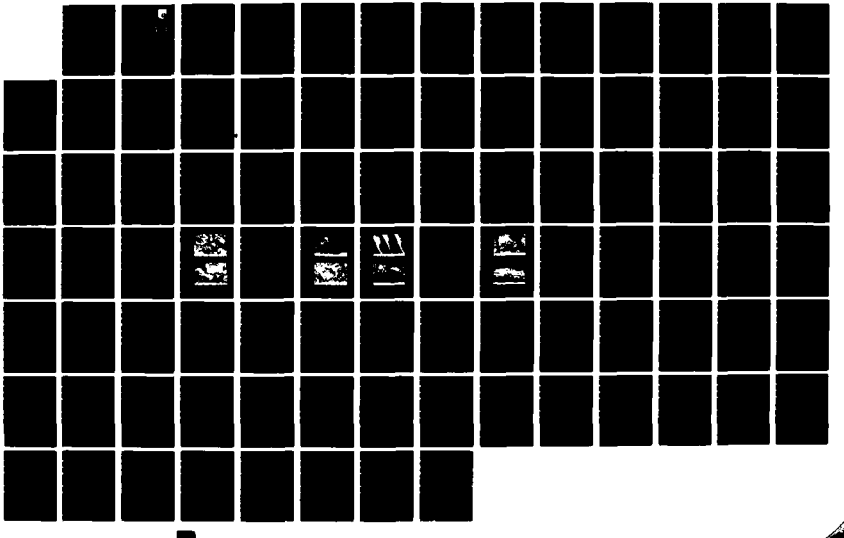

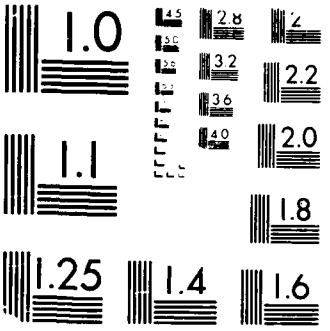

MICROCOPY RESOLUTION TEST CHART

AFWAL-TR-87-4130

THE GROWTH OF CORNER CRACKS UNDER THE CONJOINT ACTION OF HIGH AND LOW CYCLE FATIGUE

B.E. Powell, I. Henderson and R.F. Hall
Mechanical Behaviour of Materials
Department of Mechanical Engineering
Portsmouth Polytechnic
Anglesea Road Portsmouth
Hampshire PO1 3DJ England

February 1988

Final Report for Period June 1985 - June 1987

Approved for public release; distribution unlimited

MATERIALS LABORATORY
AIR FORCE WRIGHT AERONAUTICAL LABORATORIES
AIR FORCE SYSTEMS COMMAND
WRIGHT-PATTERSON AIR FORCE BASE, OHIO 45433-6533

NOTICE

When Government drawings, specifications, or other data are used for any purpose other than in connection with a definitely Government-related procurement, the United Stated Government incurs no responsibility or any obligation whatsoever. The fact that the Government may have formulated or in any way supplied the said drawings, specifications, or other data, is not to be regarded by implication, or otherwise in any manner construed, as licensing the holder, or any other person or corporation; or as conveying any rights or permission to manufacture, use, or sell any patented invention that may in any way be related thereto.

This report has been reviewed by the Office of Public Affairs (ASD/PA) and is releasable to the National Technical Information Service (NTIS). At NTIS, it will be available to the general public, including foreign nations.

This technical report has been reviewed and is approved for publication.

JOHN P. HENDERSON, Chief
METALS BEHAVIOR BRANCH
METALS AND CERAMICS DIVISION

DAVID I.G. JONES
PROJECT ENGINEER
METALS BEHAVIOR BRANCH

FOR THE COMMANDER

NORMAN M. TALLAN, Director
METALS AND CERAMICS DIVISION
MATERIALS LABORATORY

If your address has changed, if you wish to be removed from our mailing list, or if the addressee is no longer employed by your organization please notify AFWAL/MLLN , W-PAFB, OH 45433- 6533 to help us maintain a current mailing list.

Copies of this report should not be returned unless is required by security considerations, contractual obligations, or notice on a specific document.

UNCLASSIFIED
SECURITY CLASSIFICATION OF THIS PAGE

REPORT DOCUMENTATION PAGE

1a REPORT SECURITY CLASSIFICATION UNCLASSIFIED	1b RESTRICTIVE MARKINGS AD-A190 510
2a SECURITY CLASSIFICATION AUTHORITY	3 DISTRIBUTION/AVAILABILITY OF REPORT Approved for public release; distribution unlimited
2b DECLASSIFICATION/DOWNGRADING SCHEDULE	
4 PERFORMING ORGANIZATION REPORT NUMBER(S)	5 MONITORING ORGANIZATION REPORT NUMBER(S) AFWAL-TR-87 - 4130
6a NAME OF PERFORMING ORGANIZATION Mechanical Behaviour of Materials 6b OFFICE SYMBOL (If applicable)	7a NAME OF MONITORING ORGANIZATION Air Force Wright Aeronautical Laboratories, Materials Laboratory (AFWAL/MLLN)
6c ADDRESS (City, State, and ZIP Code) Portsmouth Polytechnic Hants PO1 3DJ England	7b ADDRESS (City, State, and ZIP Code) Wright-Patterson Air Force Base, OH 45433-6533
8a NAME OF FUNDING/SPONSORING ORGANIZATION Air Force Office of Scientific Research 8b OFFICE SYMBOL (If applicable) AFOSR	9 PROCUREMENT INSTRUMENT IDENTIFICATION NUMBER F49620-85-C-0116DEF
8c ADDRESS (City, State, and ZIP Code) Bolling AFB Washington, DC 20332	10 SOURCE OF FUNDING NUMBERS PROGRAM ELEMENT NO: 61102F; PROJECT NO: 2420; TASK NO: 01; WORK UNIT ACCESSION NO: 50

11 TITLE (Include Security Classification)
(U) The Growth of Corner Cracks under the Conjoint Action of High and Low Cycle Fatigue

12 PERSONAL AUTHOR(S)
B F Powell, I Henderson and R F Hall

13a TYPE OF REPORT	13b TIME COVERED	14 DATE OF REPORT (Year, Month, Day)	15 PAGE COUNT
Final	FROM 15 Jun85 TO 14 Jun87	February 1988	89

16 SUPPLEMENTARY NOTATION

17 COSATI CODES			18 SUBJECT TERMS (Continue on reverse if necessary and identify by block number) RFC
FIELD	GROUP	SUB-GROUP	Fatigue Crack Growth, Minor Cycles, da/dN Data Low/High Cycle Fatigue, Major-Minor Cycling, Ti-5331S Ti-6Al-4V
11	06		
20	11		

19 ABSTRACT (Continue on reverse if necessary and identify by block number)

Fatigue crack propagation rates have been measured for Ti-6Al-4V and Ti-5331S aeroengine disc materials using compact tension and corner notched tensile test-pieces. The loadings used simulate both the start-stop operations of aeroengines which lead to low cycle fatigue and the in-flight vibrations which may cause high cycle fatigue. It is suggested that the different fatigue crack growth behaviour of Ti-5331S, relative to that of Ti-6Al-4V, arises largely from the greater proportion of crack closure and short crack growth occurring in this alloy.

20 DISTRIBUTION/AVAILABILITY OF ABSTRACT	21 ABSTRACT SECURITY CLASSIFICATION
☒ UNCLASSIFIED/UNLIMITED ☐ SAME AS RPT ☐ DTIC USERS	Unclassified
22a NAME OF RESPONSIBLE INDIVIDUAL Dr D I G Jones	22b TELEPHONE (Include Area Code) 513-255-2689
	22c OFFICE SYMBOL AFWAL/MLLN

DD FORM 1473, 84 MAR 83 APR edition may be used until exhausted
All other editions are obsolete

SECURITY CLASSIFICATION OF THIS PAGE
UNCLASSIFIED

FOREWORD

This report was prepared by the Mechanical Behaviour of Materials Laboratory, Portsmouth Polytechnic, England, for the Metals Behavior Branch, Metals and Ceramics Division, Materials Laboratory, Air Force Wright Aeronautical Laboratories (AFWAL/MLLN), Wright-Patterson Air Force Base, Ohio, under Contract No. F49620-85-C-0116DEF, Program Element 61102F, Project No. 2420, Task No. 01, Work Unit No. 50. The work was administered under the direction of Dr D.I.G. Jones (AFWAL/MLLN) through the Air Force Office of Scientific Research (AFOSR), Bolling Air Force Base, Washington, DC, and the European Office of Aerospace Research (AFOSR), London, England. The investigation was conducted at the Mechanical Behaviour of Materials Laboratory under the leadership of Dr B.E. Powell, and the experimental study was accomplished by R.F. Hall and I. Henderson. This report describes work conducted from 15 June 1985 through 14 June 1987.

The authors wish to acknowledge the support received from the Metals Behavior Branch (AFWAL/MLLN), Wright-Patterson Air Force Base, Ohio; Rolls-Royce, Derby, and Portsmouth Polytechnic. We also wish to record our thanks to those of our colleagues who have contributed to this study in any way.

TABLE OF CONTENTS

LIST OF ILLUSTRATIONS

LIST OF ILLUSTRATIONS (CONTINUED)

LIST OF ILLUSTRATIONS (CONCLUDED)

LIST OF TABLES

SECTION 1

INTRODUCTION

The current design limitation for aeroengine discs is that of low cycle fatigue (LCF). In such rotating components the LCF loading arises from the cyclic variation of both the centrifugal and the thermal stresses. In the simplest case this major stress variation occurs once per flight. However, rotating engine components have also experienced high cycle fatigue (HCF) failures as a direct result of excessive vibrational stresses. These minor stress cycles are characterised by a high frequency and are superimposed on part of the major cycle. Consequently, in order that the fatigue integrity of these critical components might be fully assessed, it is necessary to establish the resistance of various disc and blade materials to the conjoint action of LCF and HCF loadings.

Previous studies into the effect of the conjoint action of low and high cycle fatigue, resulting from the simultaneous application of major and minor stress cycles, have clearly demonstrated the importance of high frequency, minor cycle activity(1,2). For the case of titanium-based aeroengine material containing a long through crack, the onset of this activity can be safely predicted from a knowledge of the fatigue threshold value associated with the minor cycles. Similarly, the subsequent fatigue crack growth (FCG) rates are either accurately or safely predicted by the linear summation of the individual contributions resulting from the major and minor loadings. These findings are based entirely upon test results for compact tension (CT) specimens of Ti-6Al-4V and Ti-5331S.

This investigation is concerned with the measurement of FCG rates in a corner notched (CN) specimen, since it gives a quarter-circular crack similar in shape and size to those found in aeroengine discs. The primary aim of the present study is to establish whether or not the application of major and minor cycles, either separately or in combination, results in FCG rates which can be predicted from known long through-crack behaviour.

SECTION 2

EXPERIMENTAL DETAILS

2.1 MATERIALS AND SPECIMENS

The two alloys selected for this study are the general purpose $\alpha + \beta$ alloy Ti-6Al-4V and the near-α creep resistant alloy Ti-5331S, which is also known as IMI829. These alloys show a marked contrast in terms of their microstructure, crack growth behaviour and temperature of application. Samples of both materials were cut from unused aeroengine discs. In the final stages of manufacture these discs were heat treated: the Ti-6Al-4V being solution treated at 960°C, water quenched and aged at 700°C; whilst the Ti-5331S was solution treated at 1050°C, oil quenched and aged at 650°C. As a consequence the Ti-6Al-4V consisted of regions of primary α and transformed β whose widths were approximately 25 μm, whilst the Ti-5331S possessed a prior β grain size of 0.6 mm. At room temperature the values of the 0.1% proof stress were 873 MPa and 760 MPa respectively. In addition, a small number of tests were performed on Ti-5331S material which had been further heat treated in order to develop a grain coarsened microstructure.

FCG rates for quarter-circular cracks have been determined using a corner notched test piece(3) consisting of a square sectioned bar containing a shallow notch at one corner (Fig. 1). The corner notches employed were 0.25 mm deep and 0.10 mm wide, and centrally located in test pieces with cross-sectional areas of 50 or 100 mm^2 at their gauge lengths. The orientation of the CN specimens was such that the FCG plane corresponded with the axial/tangential plane of the original disc.

2.2 TEST FACILITY

A major cycle is represented in the fatigue testing by a trapezoidal stress wave which is applied by a servohydraulic machine at a frequency of 0.1 Hz (Fig. 2a). The minor cycles are simulated by a 150 Hz sinusoidal stress wave of constant amplitude generated by an electromagnetic vibrator which is positioned between the servohydraulic actuator and the specimen. With this system the minor cycles may be superimposed upon that part of the major cycle corresponding to the cruise condition; that is the dwell on maximum load, which is extended to accommodate the required number of minor cycles (Fig. 2b).

Special specimen grips were developed for the room temperature testing of the CN specimens in the major-minor cycling test facility. Three problems were resolved in the final grip design. First, the correct operation of a crack monitoring system involving the direct current potential drop (DCPD) technique requires at least one end of the gripping arrangement to be electrically insulated. This difficulty was overcome by locating a reinforced phenolic resin insert and washer arrangement between the upper grip and collar as shown in

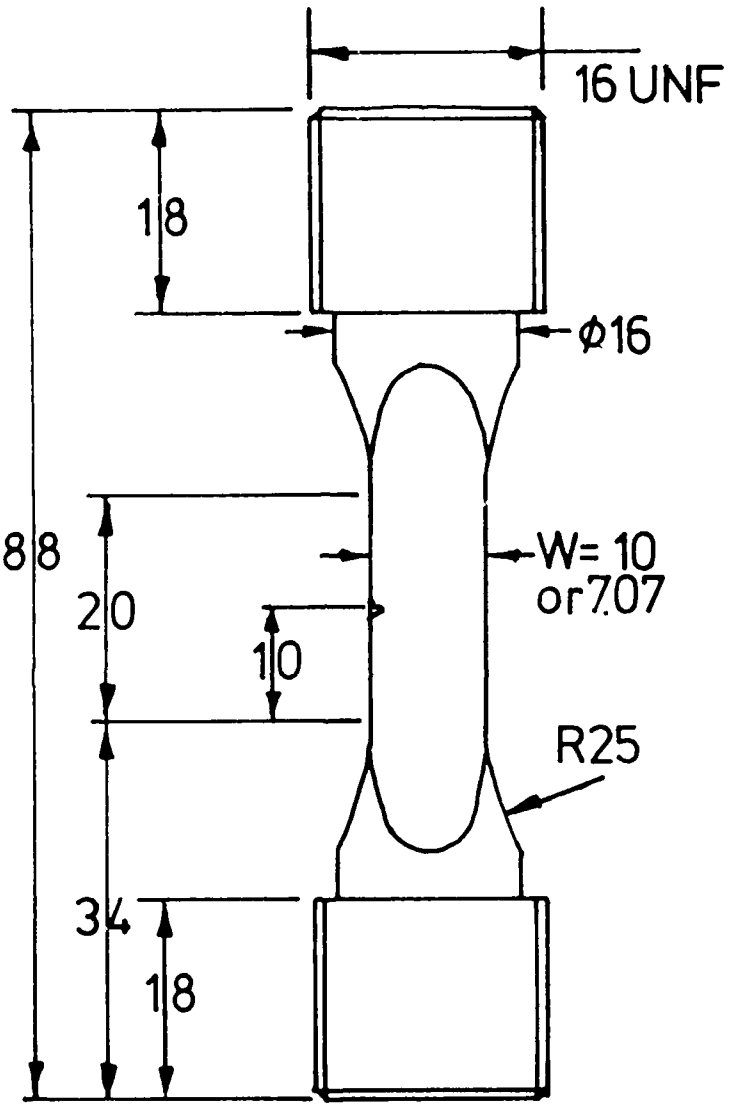

Fig. 1. Corner Notched Specimen

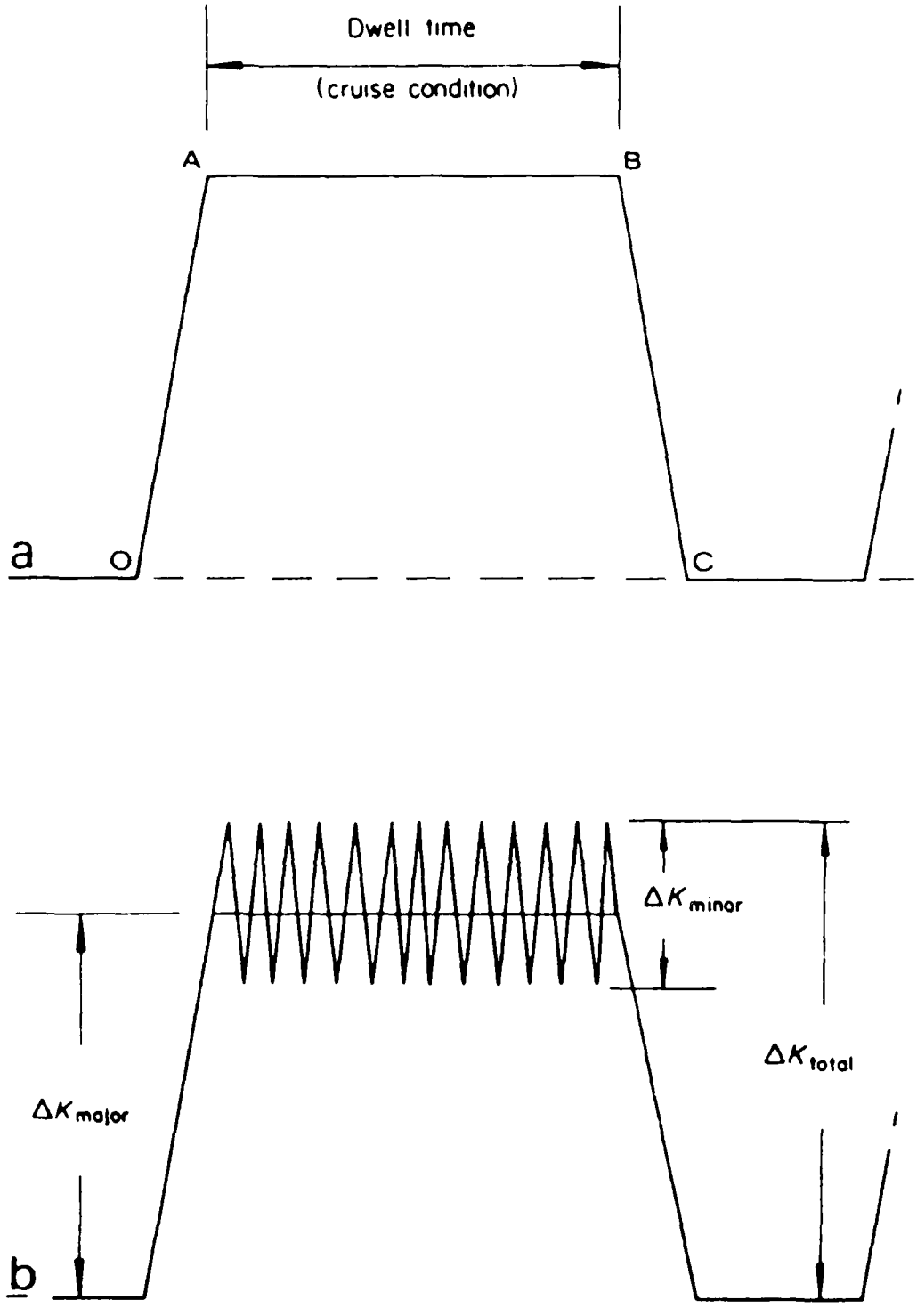

Fig. 2. Terminology for major-minor cycling; (a) major cycle only, (b) combined major and minor cycles

Fig. 3. The second problem was that of inserting and subsequently removing from the grips specimens which have threaded ends. Normally servohydraulic actuators are free to rotate about their major axis, but in the major-minor cycling rig the pull rod, which is attached to the table of the electromagnetic vibrator, is preloaded in such a manner as to inhibit this motion. However, the required rotational movement is provided in the design by allowing the upper grip to rotate within the collar during specimen loading and removal; this movement being prevented during testing by the upper grip lock nut. Finally, it was considered essential that the design facilitated the loading and removal of specimens without movement of the load frame crosshead. This problem was solved by allowing sufficient vertical movement of the upper grip within the collar once the lock nut was undone. An effective grip design was achieved despite severe height restrictions, and grips manufactured from a high tensile steel proved to be entirely satisfactory.

Using a CN specimen as a bending dynamometer, and with a strain gauge mounted centrally on each of the four faces, the position of the upper grip was adjusted until the alignment conformed to the ASTM specification for axial load fatigue machines(4). This specification requires that the bending of the strain gauged specimen must be minimised in such a way that the strain measured by any individual gauge does not differ by more than 5% from the average strain measured by all the gauges on the specimen.

Subsequently the static and dynamic load calibrations of the major-minor cycling rig were obtained again using a dynamometer based upon the CN test specimen design. The static loads applied by the servohydraulic actuator of the test machine agreed within 0.5% with those given by a certified British Standard grade A tensile machine. The method used for the calibration of the minor cycles used a Vishay strain bridge amplifier which has a proven dynamic testing capability, together with a high quality oscilloscope. Using this system, static and dynamic signals were compared over the working range of the electromagnetic vibrator, and it was found that the dynamic loads achieved were greater than expected by a consistent amount. This discrepancy is solely due to the existence of a residual dynamic load which is apparent when the minor cycle load is set to zero. Such a response is an essential characteristic of a stable minor cycle control system, for it is necessary to apply a small positive offset voltage to the minor cycle control circuit to prevent the electronic noise generating a condition of positive feedback. Consequently, the transfer function between the dynamic loads demanded and those achieved was carefully established and periodically confirmed throughout the test programme.

2.3 CRACK LENGTH MEASUREMENT

The application of fracture mechanics to fatigue crack propagation is dependent on the accurate meaurement of both absolute values and relative changes of crack length. A plastic replication technique is suitable for the measurement of short crack lengths (< 0.6 mm) during

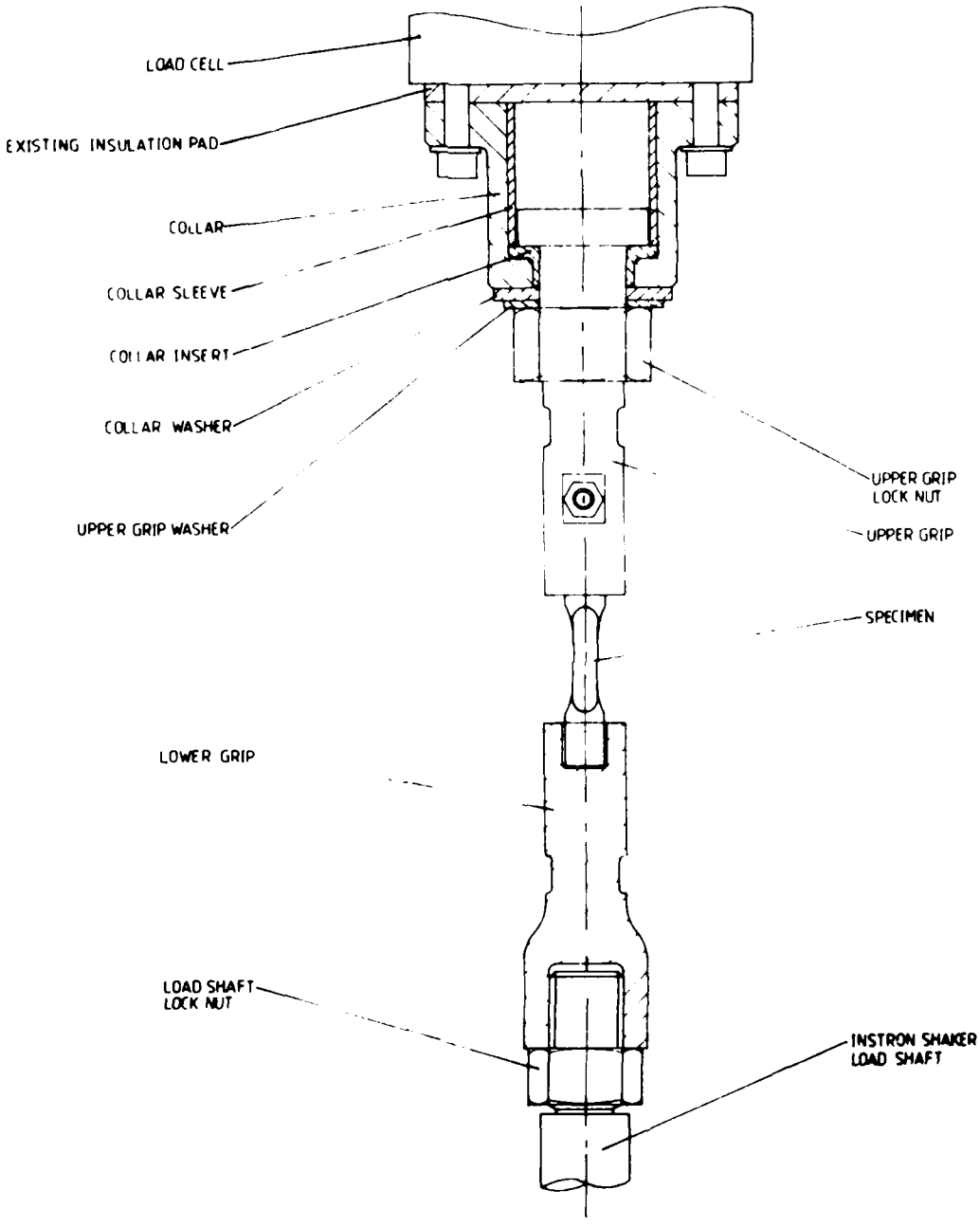

Fig. 3. CN Specimen Grip Design

precracking, whilst a DCPD system is preferred for monitoring the subsequent period of crack growth. The replication process is also used to define the initial and final surface crack lengths associated with the use of the DCPD system.

In the replication process, a small piece of cellulose acetate sheet, 35 μm thick, is dipped in acetone, and placed on the side of the specimen covering the notch. After a period of 2-5 minutes the replica can be detached from the specimen, mounted on a glass slide, and examined under an optical microscope at x 100 magnification. A scale in the micrometer eyepiece enables the crack length from the notch to be measured with a precision of 0.01 mm.

The DCPD technique of crack measurement is a widely accepted method of monitoring fatigue crack growth. The method is based on an increase of resistance due to the reduction in area which accompanies crack advance. By passing a constant current through the specimen the voltage increase across the crack plane, due to this area reduction, can be monitored as the test proceeds. Voltage is then related to crack length by means of a calibration for the appropriate specimen.

The DCPD calibration employed for the CN specimens was that obtained by Hicks and Pickard(3) using a 3-dimensional finite element analysis. Apart from the initial section of the calibration, the voltage varies linearly with crack length. The extent of the non-linear portion is a function of the probe spacing at the notch, being reduced by a low ratio of voltage probe spacing (Z) to specimen width (W). A Z/W ratio of 0.025-0.03 is obtained with a 10 x 10 mm CN specimen, thereby limiting the non-linear calibration to the first 0.5 mm of crack growth.

In order to measure and negate thermoelectric effects, a pulsed DCPD system has been developed for the crack growth testing of CN specimens. The pulsing of the 30A current and the recording of the notch and reference potentials are automatically determined by a microprocessor controlled data logger. Both potentials are recorded during every major cycle dwell period, first with the current off and then with the current on. Thus, the ratio of the voltage at the notch to the reference voltage (V_c/V_{ref}), suitably corrected for thermoelectric effects, may be calculated within the data logger using the relationship:

$$\frac{V_c}{V_{ref}} = \frac{V_c(on) - V_c(off)}{V_{ref}(on) - V_{ref}(off)} \quad \ldots\ldots (1)$$

where,

$$\frac{V_c(on)}{V_c(off)} = \frac{\text{notch voltage current on}}{\text{notch voltage current off}}$$

$V_{ref(on)}$ = reference voltage current on

$V_{ref(off)}$ = reference voltage current off

Each calculated value is temporarily stored within the logger, and periodically an average value is printed; the frequency of data output depending on the rate of crack growth.

2.4 TEST METHOD

Each CN specimen is precracked under load control by a 3 Hz sinusoidal waveform at a stress ratio of 0.1. The precracking schedule must generate a crack whose behaviour is independent of its prior loading history, and whose length is 0.5 0.6 mm. In addition, the process should generate within the specimen a level of stress intensity which is 3-4 MPa$\sqrt{m}$ below the anticipated value of ΔK_{onset}, this parameter corresponding to the minimum condition necessary for minor cycle crack growth. For tests involving a ratio of minor to major amplitudes of 0.12 it is sufficient to apply loads of 2.5 - 25 kN for they generally result in the formation of a crack within 30 000 cycles, and when the precrack is grown to a length within the prescribed limits the prevailing level of ΔK is the required value of approximately 14 MPa$\sqrt{m}$. Similarly, a ΔK of approximately 3 MPa$\sqrt{m}$ is required before tests involving an amplitude ratio of 0.22 can commence. Table 1 shows the loadings employed in this case for a CN specimen of 50 mm^2 cross-section, together with the crack lengths and stress intensity ranges achieved at the end of each step of the precracking schedule. The load reductions at the first and second steps are 30 and 20%, whilst the subsequent crack growth increments correspond to 1 and 3 times the plastic zone sizes calculated for loading conditions of monotonic plane stress.

Table 1 Precracking schedule for tests at Q = 0.22. Loadings for a CN specimen of 50 mm^2 cross-sectional area

Step	Maximum Load (kN)	Minimum Load (kN)	Final Crack Length (mm)	Final ΔK (MPa$\sqrt{m}$)
Crack Formation	2.50	25.0	0.40	11.7
First Step-Down	1.75	17.5	0.48	8.9
Second Step-Down	1.40	14.0	0.60	8.1

Using an inspection interval of 2500 cycles, and maintaining the static mean load level, each specimen is inspected by the replication technique until a crack is detected. Thereafter the inspection interval is progressively decreased, until the crack length, including the notch depth, lies between 0.5 and 0.6 mm. At this stage, the final precrack length is noted, and the specimen is removed from the fatigue machine for the attachment of the DCPD probes.

Reference probe positions, as shown in Fig. 4, are marked on the specimen using a vernier height gauge. The voltage probes are constructed from short lengths of 0.05 mm diameter platinum wire welded to the specimen by means of a constant voltage welding set fitted with a parallel gap welding head and a specimen holding jig giving controlled movement of the specimen in three orthogonal directions.

The specimen is carefully reloaded into the test rig, and the DCPD probe wires connected to the data acquisition equipment. A period of 12 hours is allowed for the stabilisation of the temperature within the surrounding environmental chamber. After this time the load cell settings are checked, the initial DCPD voltage ratio established, and the crack allowed to grow under the chosen loading conditions.

Each test is terminated at a ratio of crack length to specimen width (a/W) between 0.5 and 0.6, the final voltage ratio being recorded. In addition, the final surface crack lengths are measured both on the loaded specimen with acetate replicas, and subsequently with a toolmaker's microscope.

2.5 ANALYSIS OF DATA

Following the cessation of the test, the output from the data logger, recorded on the strip printer, is inspected to find the number of major cycles corresponding to increments of 0.2 in the observed voltage ratio. A value of 0.2 gives a suitable number of data points whilst ensuring that the minimum increment in crack length is substantially greater than the crack length measuring precision(5). The DCPD calibration, used to convert the selected voltage ratios to crack lengths, is based upon a linear interpolation between the two known surface crack lengths and corresponding voltage ratios, established at the termination of the precracking and testing stages. Growth rates are determined by the 3-point secant method.

Stress intensity calibrations, which can be used for the CN specimen, have been developed by Pickard(6) using a 3-dimensional finite element analysis. He indicates that the stress intensity for a crack with an elliptical crack front can be expressed in the form:

$$K = M_G.M_B.M_S.F(\sigma).\Phi.(\pi a)^{1/2} \qquad \ldots\ldots (2)$$

Where M_G is a general correction factor, M_B is a back-face correction factor, M_S is a side face correction factor, $F(\sigma)$ is a stress function

R : DCPD Reference Probes

N : DCPD Notch Probes

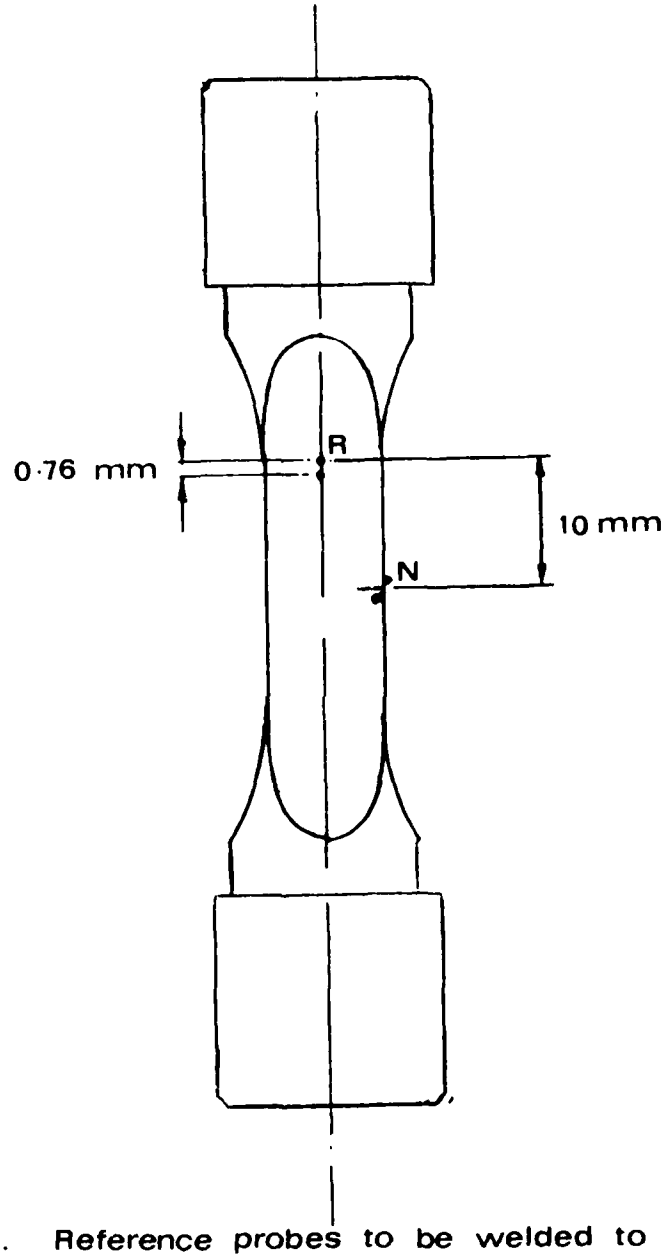

N. B. Reference probes to be welded to one face that is NOT adjacent to the notch

Fig. 4. CN specimen PD probe locations

related to the remote stress distribution, Φ is the standard elliptical correction factor, and a is the crack length.

The correction factors M_G, M_B and M_S depend on the form of crack being analysed (i.e., corner, surface or subsurface), and on the position being analysed along the crack front. For a corner crack at the surface position, the correction factors are:

$$M_G = 1.143 \quad (0 \leq x \leq 0.2) \qquad \ldots\ldots (3)$$

$$M_G = 0.1x^2 + 0.29x + 1.081 \quad (0.2 < x \leq 0.75) \qquad \ldots\ldots (4)$$

$$M_B = 1 + 0.06x \quad (0 \leq x \leq 0.2) \qquad \ldots\ldots (5)$$

$$M_B = 0.75x^2 - 0.185x + 1.019 \quad (0.2 < x \leq 0.75) \qquad \ldots\ldots (6)$$

$$M_S = 1 + 0.07x \quad (0 \leq x \leq 0.2) \qquad \ldots\ldots (7)$$

$$M_S = 0.9x^2 - 0.21x + 1.020 \quad (0.2 < x \leq 0.75) \qquad \ldots\ldots (8)$$

where,

$$x = a/W$$

For the case of a CN specimen, $F(\sigma)$ is equal to the remote tensile stress given by P/W^2, where P is the applied load, whilst the value of the standard elliptical correction factor is $2/\pi$. Thus equation 2 may be written as:

$$K = \frac{2\ AP\ (\pi a)^{1/2}}{\pi W^2} \qquad \ldots\ldots (9)$$

Where A is the product of the correction factors: M_G, M_B and M_S, for the appropriate crack front position. The stress intensity value associated with a quarter circular crack front is a maximum at the surface of the specimen, and in this report all the stress intensity values related to FCG rates are for this location.

Finally the crack growth rates (da/dN) are plotted as a function of the controlling parameter ΔK using logarithmic co-ordinates. In tests which involve major cycles only, the identification of N and ΔK is unambiguous. In representing crack growth results involving the conjoint action of major and minor stress cycles it is necessary to define what constitutes one cycle and also, which stress intensity range is to be considered. In this case each loading block contains one major cycle which represents an engine flight, the obvious countable event used in assessing the life of engine components subjected to low cycle fatigue. At the same time the overall or total stress

intensity range (ΔK_{total}) is that experienced by a cracked component subjected to the conjoint action of the two stress cycles (Fig. 2b). Growth rates due to combined major and minor cycles are, therefore, identified by the symbol da/dblock and presented as a function of ΔK_{total}.

2.6 MICROSTRUCTURALLY SHORT CRACK EXPERIMENTS

Exploratory experiments have been conducted using CN test pieces of deliberately grain coarsened Ti-5331S in order to emphasis the short crack growth regime and its possible effect upon the FCG rates under combined high and low cycle fatigue.

Grain coarsening consisted of heating the test pieces to 1250°C for 24 hours in vacuum and cooling in two stages, to 600°C in the furnace, then air cooled to room temperature. This was followed by reheating to 550°C in air for 24 hours followed by air cooling to room temperature. The grain size was thereby increased from approximately 0.6 mm to 2 mm.

Some oxidation and thermal etching of the test piece surface occurred, which had to be removed before testing commenced in order that cracking would be clearly visible on the surface, and reliable acetate replicas taken. For this reason the test pieces were metallographically polished on the two faces where cracks would appear on the surface. Polishing was accomplished by lightly cleaning the surface with fine grade emery paper followed by increasing fineness in lapping paste. To enable the microstructure to be visible, the surfaces were etched with a solution of 2% HF/10% HNO_3 in water.

The size of the notch on both faces of each test piece was measured using an optical microscope. Precracking of the test pieces in the testing machine consisted of subjecting them to sinusoidal loading in tension between 2 and 20 kN at 3 Hz until a crack broke out of the notch on to one or both surfaces.

Fatigue loadings applied to the test pieces were either major cycles or minor cycles alone or a combination of both. Apart from solely minor cycle loading, the maximum and minimum applied loads were the same as those used for precracking. After appropriate periods of fatigue cycling, test pieces were inspected at a magnification of x 100 and the distribution of surface cracks noted. At the same time acetate replicas of both surfaces were taken and used to measure the length of the crack. It was found that considerable crack branching occurred, as a consequence the crack length was recorded as the sum of the notch depth and the distance from the notch root to the furthest crack tip, measured in a direction perpendicular to the direction of stressing. Testing continued until a crack had grown approximately half way across the test piece.

Analysis of the data obtained from the tests involved determining (i) the stress intensity at the crack tip, assuming that the crack progressed through the material in the form of a true quarter circle;

(ii) the FCG rate using the three point secant method; and (iii) where relevant, the onset of minor cycle crack propagation. In compiling and analysing the results the two crack faces of each test piece were treated in two ways; separately and in combination.

2.7 FRACTOGRAPHY

A Jeol 35M scanning electron microscope was used to obtain magnified images of the fracture surfaces. The machine was operated in the emissive mode, using the intermediate objective aperture and a potential difference in the electron gun of 20 to 25 kV. Each specimen sample was loaded into the microscope and, without tilting relative to the electron beam, orientated with respect to the machine's traversing micrometers. Two traverses across the crack surface from the corner notch were made, one towards the diagonally opposite corner and the other parallel and close to one edge of the specimen. This progression from the notched corner enabled changes in surface characteristics to be observed as a function of crack length and hence the stress intensity range.

Photographs of the fatigue crack surface were taken at approximately 0.5 mm (0.02") intervals along both traverses. In general a magnification of 600 - 1000x was used. As each photograph was taken, the readings of the two traversing micrometer verniers were noted to give co-ordinates for the photographic frame. These co-ordinates, in conjuction with the co-ordinates for the notched corner of the specimen, were used to calculate the length of crack and hence the stress intensity at that point. Pickard's solution (6, 7) of stress intensities for quarter circular cracks loaded in remote tension have been used to calculate the value of applied ΔK or ΔK_{total}, for both the diagonal and edge positions on the crack front. These solutions were used as the basis for assessing variations in the morphology of the fatigue crack surface.

SECTION 3

FATIGUE CRACK GROWTH IN DISC MATERIALS

3.1 LOW CYCLE FATIGUE CRACK GROWTH

Table 2 lists the loading conditions used in each FCG test performed on CN specimens. Where separate major or minor stress cycles were employed the stress ratio (R) is indicated. The parameter used to describe the relative magnitude of the combined stress cycles is the amplitude ratio (Q) defined as the ratio of minor to major stress amplitudes. For a cracked component this corresponds to the ratio of the minor to major stress intensity ranges. Similarly, the cycle ratio (n) indicates the relative number of minor and major stress cycles, and this parameter corresponds to the number of minor cycles per loading block. The stress ratio of the minor cycles (R_{minor}) can be related to the major cycle stress ratio and the amplitude ratio. Thus, by equating expressions for the mean stress of the minor cycles and the maximum stress of the major cycle, it may be shown that:-

$$R_{minor} = \frac{2 - Q\ (1 - R_{major})}{2 + Q\ (1 - R_{major})} \qquad \ldots\ldots\ (10)$$

For the test conditions of $R_{major} = 0.1$ and $Q = 0.22$ and 0.12, the minor cycle stress ratios are 0.82 and 0.90.

Table 2 Summary of test conditions

Specimen Number	Alloy	Condition	Loading
A1	Ti-6Al-4V	Disc Material	Major cycles only, R = 0.1
A2	Ti-6Al-4V	Disc Material	Major cycles only, R = 0.1
A3	Ti-6Al-4V	Disc Material	Q = 0.12, n = 10 000
A4	Ti-6Al-4V	Disc Material	Q = 0.12, n = 10 000
A5	Ti-6Al-4V	Disc Material	Q = 0.22, n = 1 000
A6	Ti-6Al-4V	Disc Material	Q = 0.22, n = 1 000
B1	Ti-5331S	Disc Material	Major cycles only, R = 0.1
B2	Ti-5331S	Disc Material	Major cycles only, R = 0.1
B3	Ti-5331S	Disc Material	Q = 0.12, n = 10 000
B4	Ti-5331S	Disc Material	Q = 0.12, n = 10 000
B5	Ti-5331S	Disc Material	Q = 0.22, n = 1 000
B6	Ti-5331S	Disc Material	Q = 0.22, n = 1 000

Specimen Number	Alloy	Condition	Loading
C1	Ti-5331S	Grain Coarsened	Majors only, R = 0.1
C2	Ti-5331S	Grain Coarsened	Minors only, R = 0.82
C3	Ti-5331S	Grain Coarsened	Q = 0.12, n = 1 000
C4	Ti-5331S	Grain Coarsened	Q = 0.22, n = 1 000
C5	Ti-5331S	Grain Coarsened	Q = 0.22, n = 1 000

Major cycle FCG rates corresponding to stress intensity ranges above 15 MPa√m have been measured for Ti-5331S disc material and compared with those for Ti-6Al-4V disc material (Fig. 5). The greater scatter in the results for Ti-5331S is a characteristic feature of this near α titanium alloy, nevertheless the observed growth rates fall within the wide scatter band reported by Duncan et al(8) for room temperature FCG rates in this alloy. At all levels of stress intensity range examined the Ti-5331S exhibited slower FCG rates, which is consistent with the behaviour observed previously using CT specimens(2). The differences in the major cycle growth rates of Ti-6Al-4V and Ti-5331S were reconciled by the use of an effective range of stress intensity (2).

The FCG rates in CT and CN specimens of Ti-6Al-4V subjected solely to major cycle loadings are in agreement for $\Delta K \lesssim 20$ MPa√m. Above this level, slower rates of growth are associated with the CN specimen. This behaviour (Fig. 6) is the same as that reported elsewhere both for Ti-6Al-4V(9) and nickel-based superalloys(10). However, the results obtained for the alloy Ti-5331S are in contrast to these findings, since the growth rates observed in the two types of specimen are essentially the same at all levels of ΔK examined (Fig. 7).

3.2 FATIGUE CRACK GROWTH DUE TO COMBINED HIGH AND LOW CYCLE FATIGUE

The rates of FCG in CN specimens of Ti-6Al-4V subjected to combined major and minor stress cycles has been measured for the following combinations of amplitude ratio and cycle ratio:

(1) Q = 0.12, n = 10 000

(2) Q = 0.22, n = 1 000

The repeatable results shown by duplicate tests are apparent in Figs. 8 and 9.

It was considered that the chosen test conditions would give practical rates of FCG due to the overall major cycle when ΔK_{total} was less than

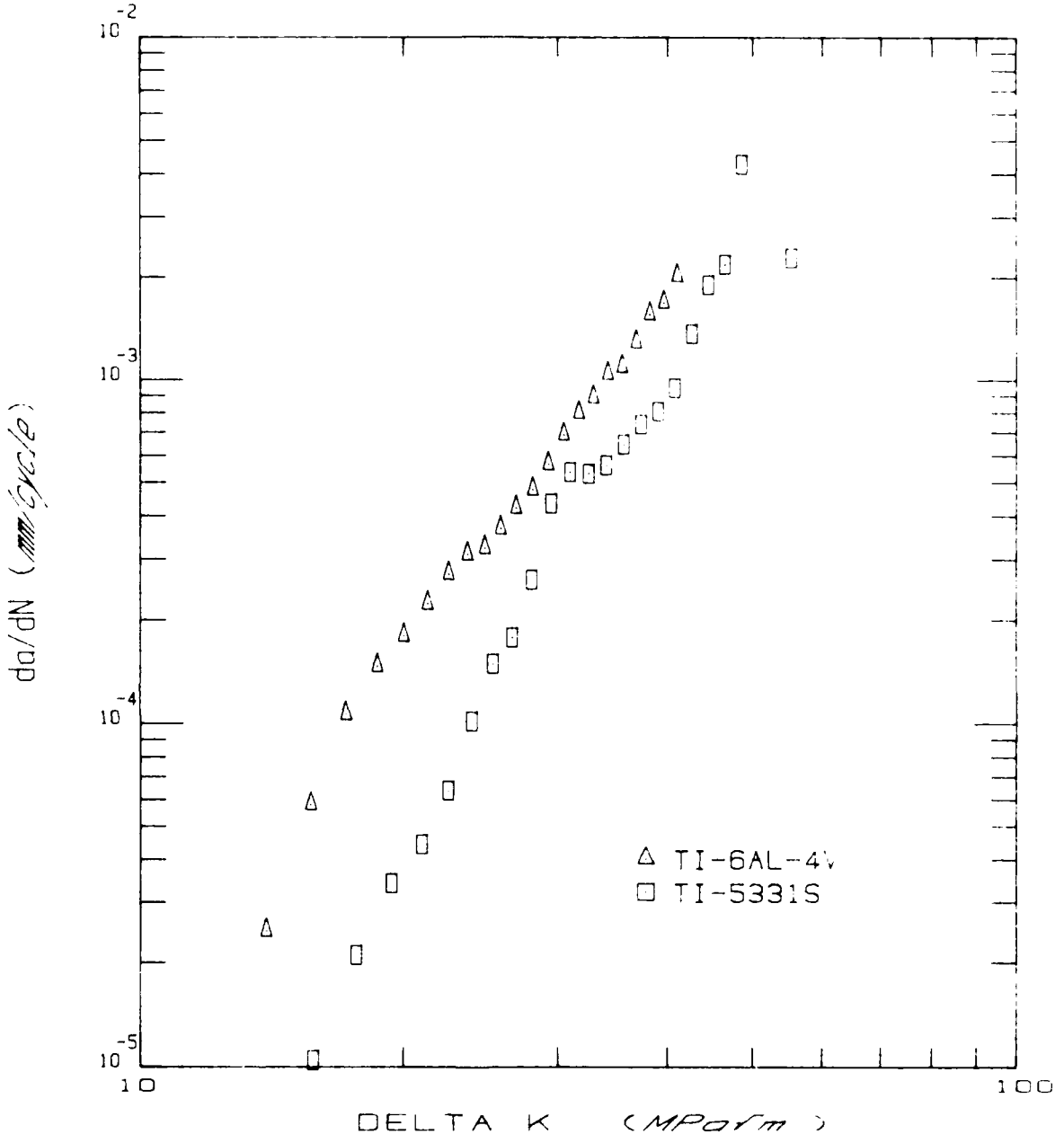

Fig. 5. Comparison of major cycle FCG rates for corner cracks in Ti-6Al-4V and Ti-5331S

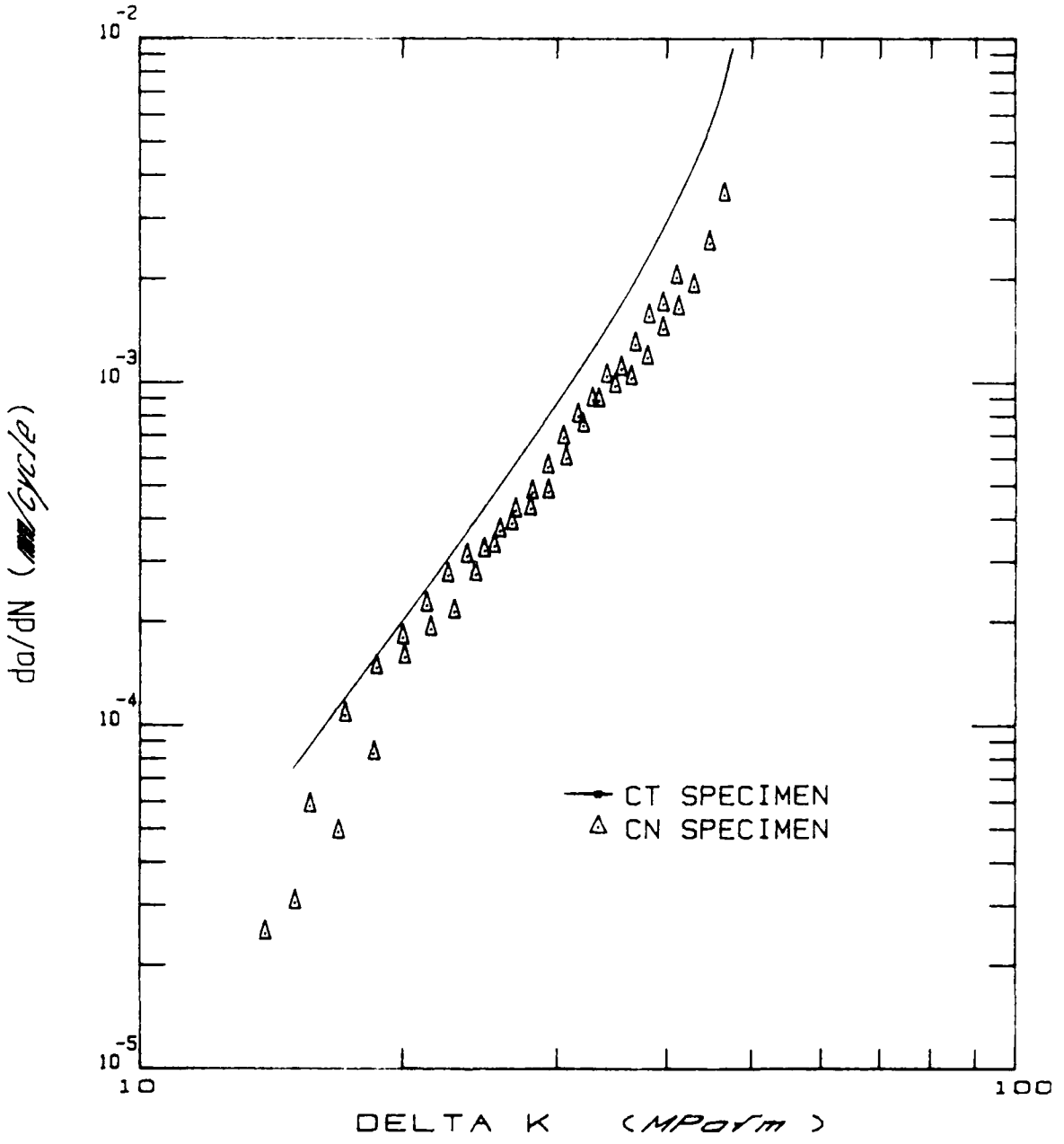

Fig. 6. Comparison of major cycle FCG rates for Ti-6Al-4V in CN and CT Specimens

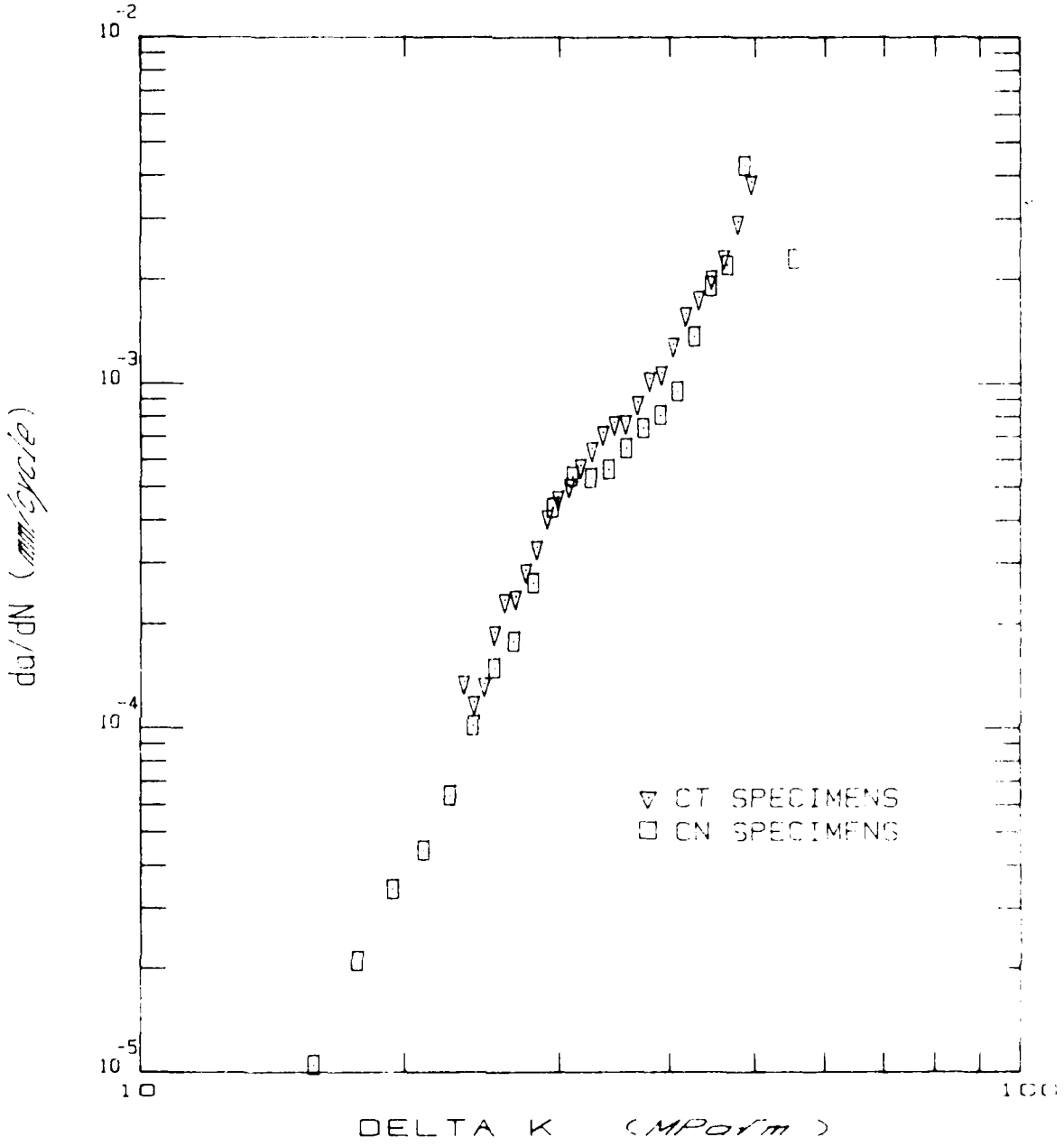

Fig. 7. Comparison of major cycle FCG rates for Ti-5331S in CN and CT specimens

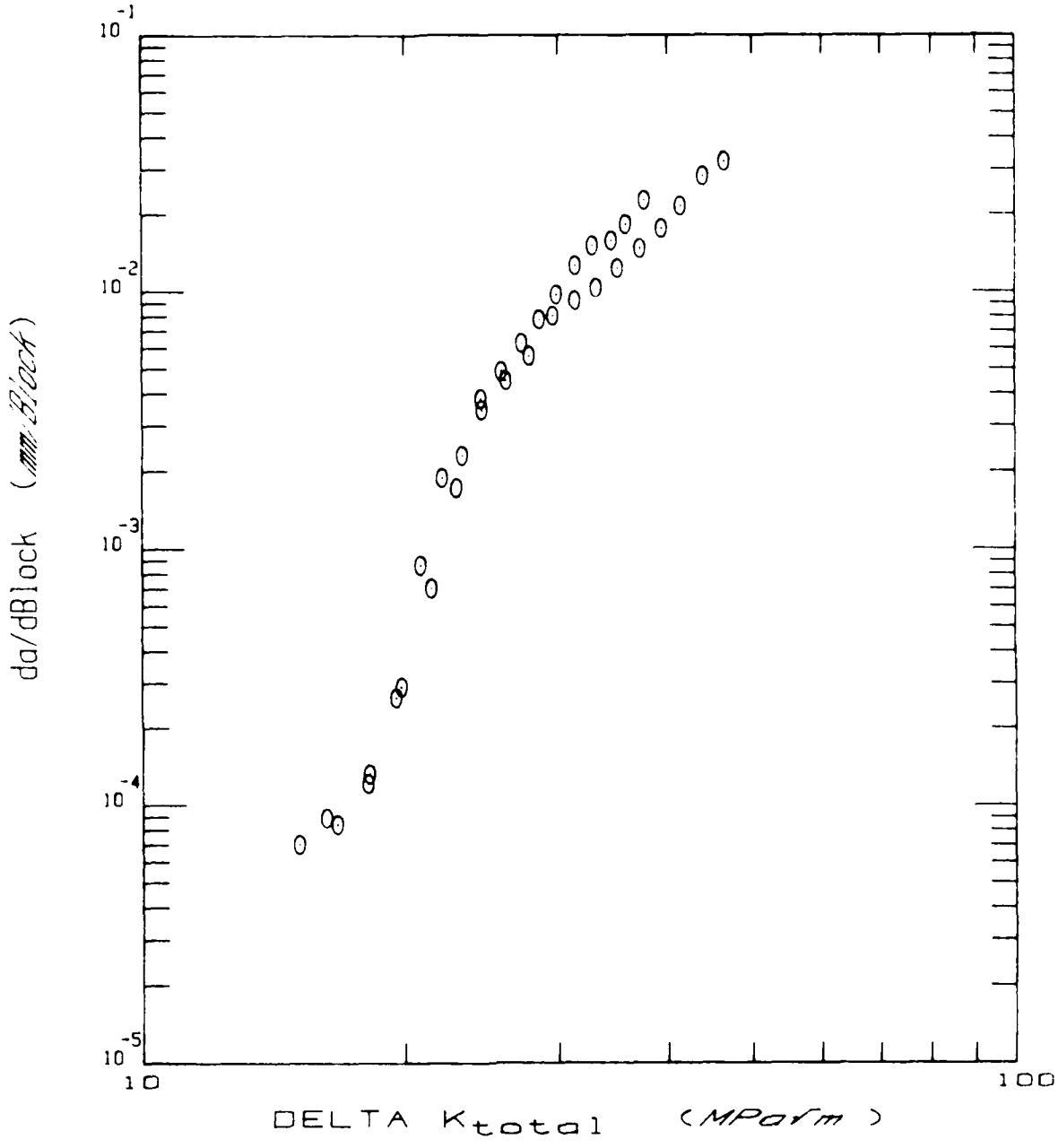

Fig. 8. FCG rates in CN specimens of Ti-6Al-4V at an amplitude ratio of 0.12 and a cycle ratio of 10 000 (duplicate tests)

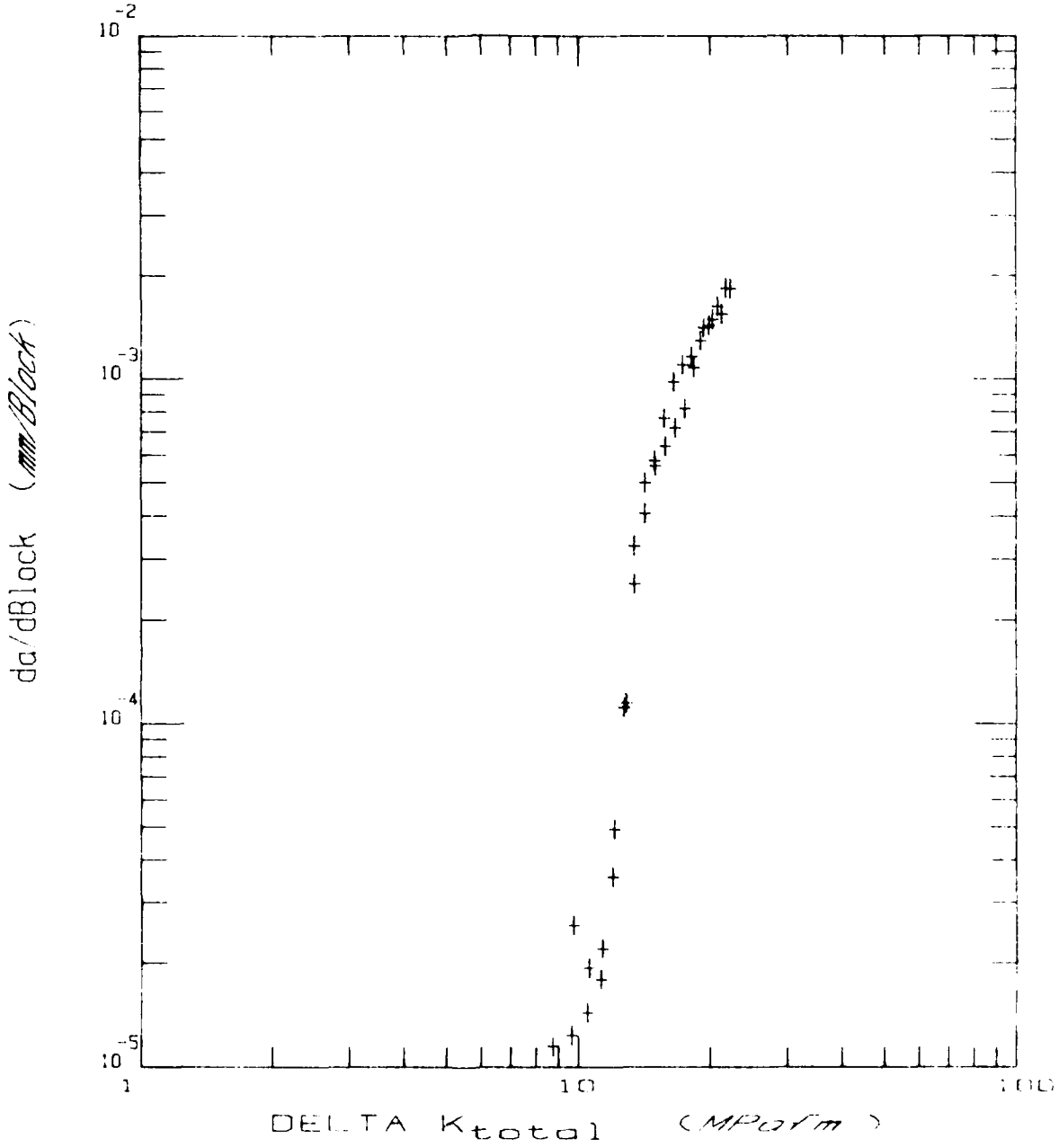

Fig. 9. FCG rates in CN specimens of Ti-6Al-4V at an amplitude ratio of 0.22 and a cycle ratio of 1000 (duplicate tests).

ΔK_{onset}, whilst ensuring a marked change in growth rate following the onset of minor cycle crack growth. This proved to be the case, as indicated in Figs. 10 and 11. Here the measured FCG rates are compared with those generated by major cycles alone. The agreement between the two sets of data at low stress intensity ranges, and the subsequent divergence of the data, are apparent in each case. An estimate of ΔK_{onset} can be obtained from such figures by taking ΔK_{onset} to be the value of ΔK_{total} intermediate between the greatest value at which the two sets of data agree and the lowest value at which they clearly diverge. Although this is only a simple approach to the estimation of ΔK_{onset} from the available growth rate data, it corresponds closely to that used in the analysis of previous tests on CT specimens.

Estimates of ΔK_{onset} obtained by this method for CN specimens of Ti-6Al-4V are shown in Table 3, where two comparisons are made. The first comparison is with predictions of ΔK_{onset} based upon threshold data obtained from CT specimens(2) whilst the second comparison is with ΔK_{onset} values established for long through crack growth in CT specimens(2). In each case the correlation is good.

TABLE 3 Comparison of predicted and experimental values of ΔK_{onset} for Ti-6Al-4V

Amplitude Ratio	ΔK_{onset} MPa$\sqrt{m}$		
	Predicted From Threshold Values	Experimental, CT Specimens	Experimental, CN Specimens
0.12	18.5	18.8 ± 0.7	19.0 ± 0.8
0.12	18.5	18.5 ± 0.5	18.9 ± 0.7
0.22	11.9	12.1 ± 0.3	11.7 ± 0.3
0.22	11.9	12.2 ± 0.3	11.6 ± 0.4

The close agreement between the results from the two specimen designs is not limited to the onset of minor cycle activity under a combined loading of major and minor stress cycles. Figs. 12 and 13 clearly show that the FCG rates measured in CT and CN specimens after the onset of minor cycle growth are essentially the same.

The rates of FCG in CN specimens of Ti-5331S subjected to combined major and minor stress cycles has been measured using the same combinations of amplitude ratio and cycle ratio applied to Ti-6Al-4V. The repeatable results shown by duplicate tests are apparent in Figs. 14 and 15.

On the basis of the results for Ti-6Al-4V it was considered that the

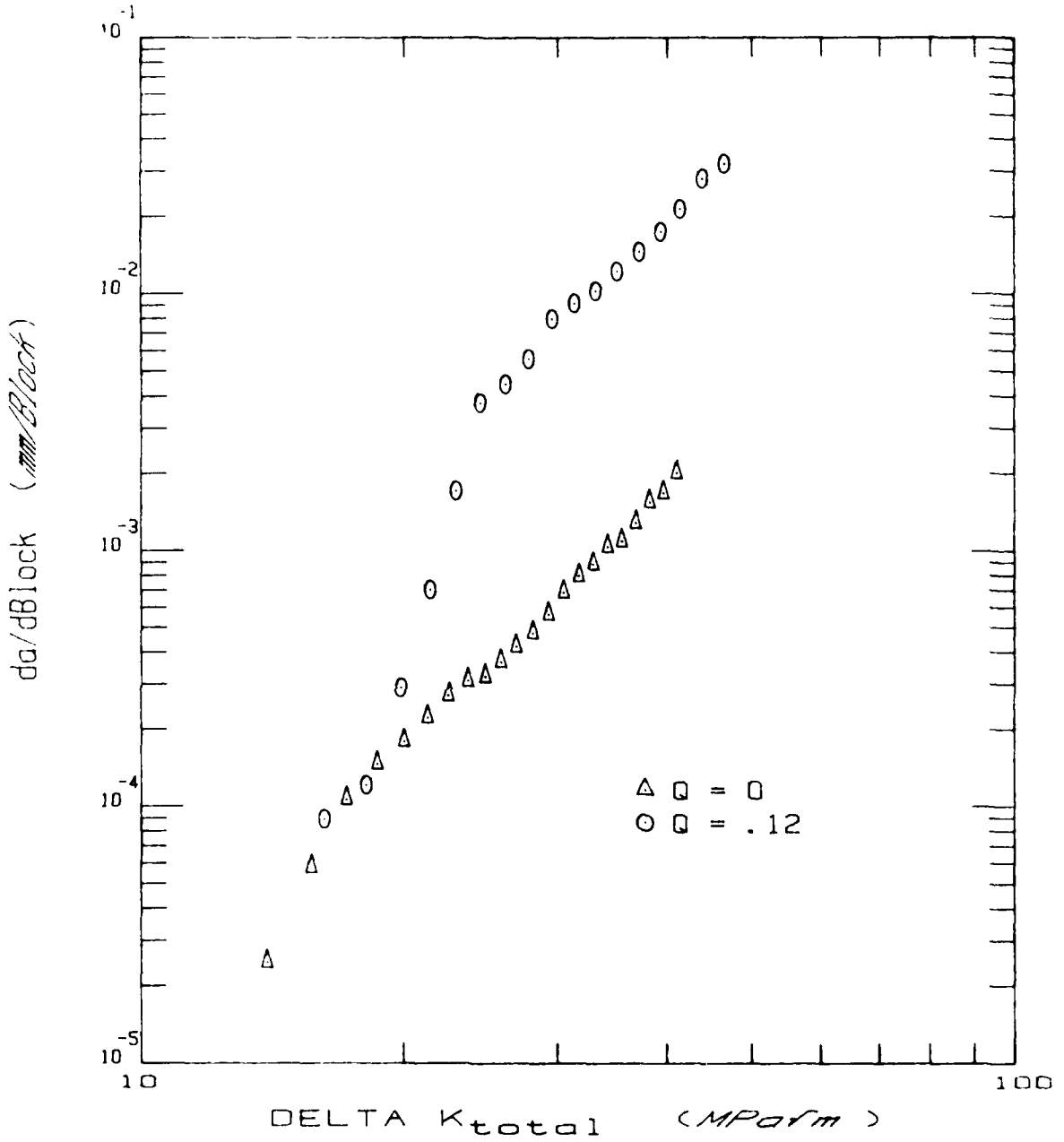

Fig. 10. Comparison of FCG rates for CN specimens of Ti-6Al-4V for major cycles only (Q = 0) and combined major and minor stress cycles (Q = 0.12 and n = 10 000)

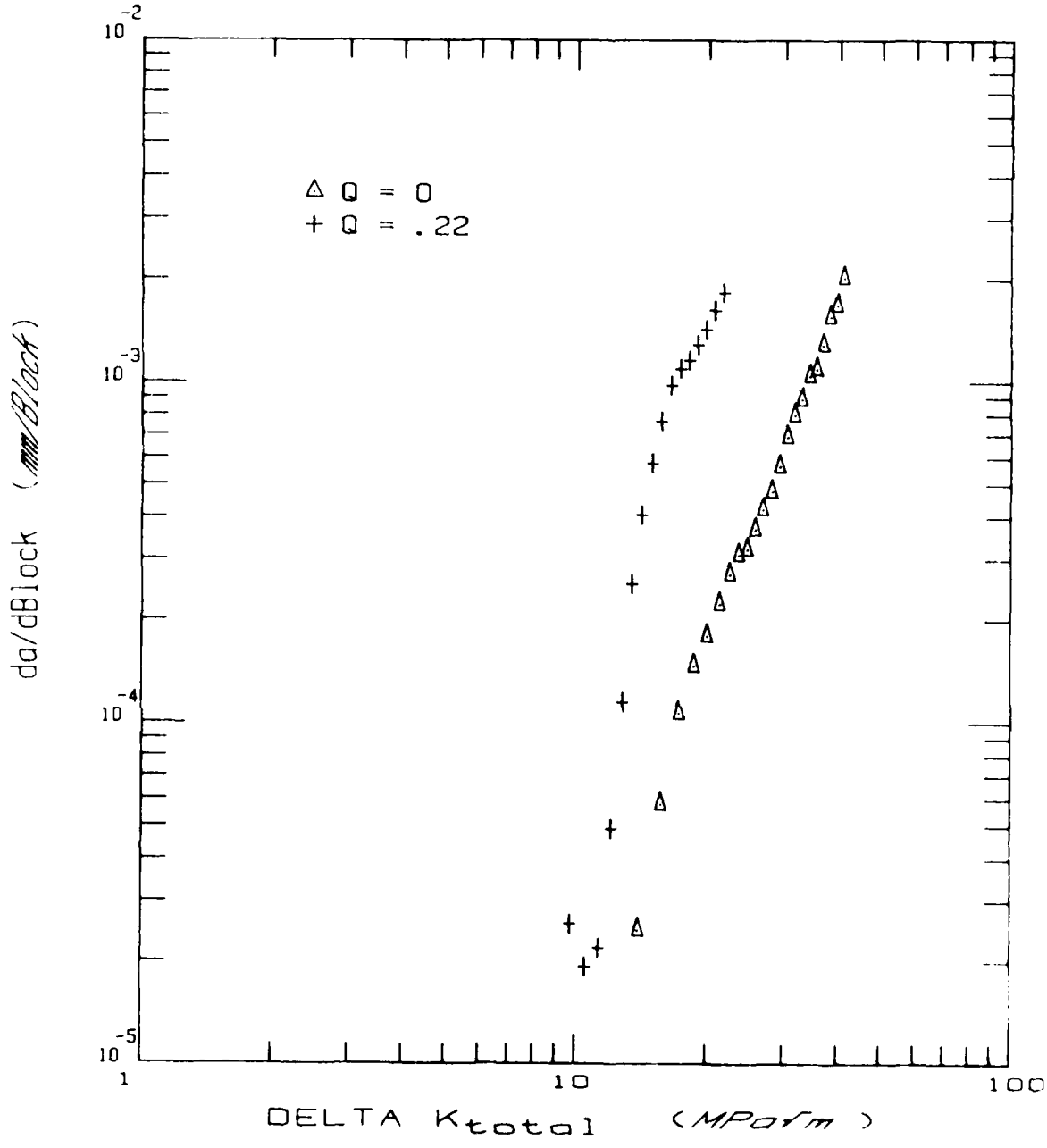

Fig. 11. Comparison of FCG rates for CN specimens of Ti-6Al-4V for major cycles only (Q = 0) and combined major and minor stress cycles (Q = 0.22 and n = 1000)

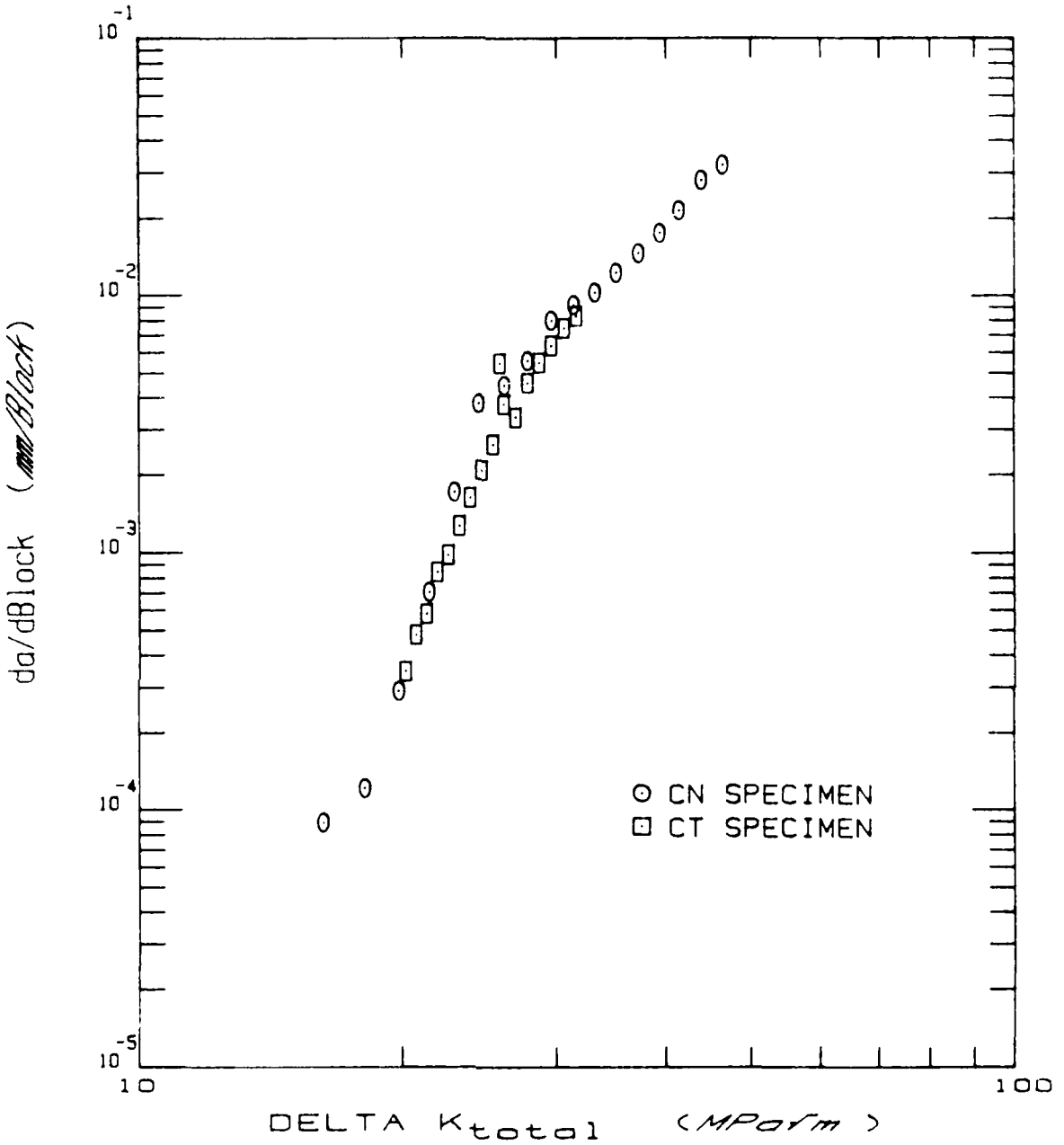

Fig. 12. Comparison of FCG rates in Ti-6Al-4V for CN and CT specimens at an amplitude ratio of 0.12 and a cycle ratio of 10 000

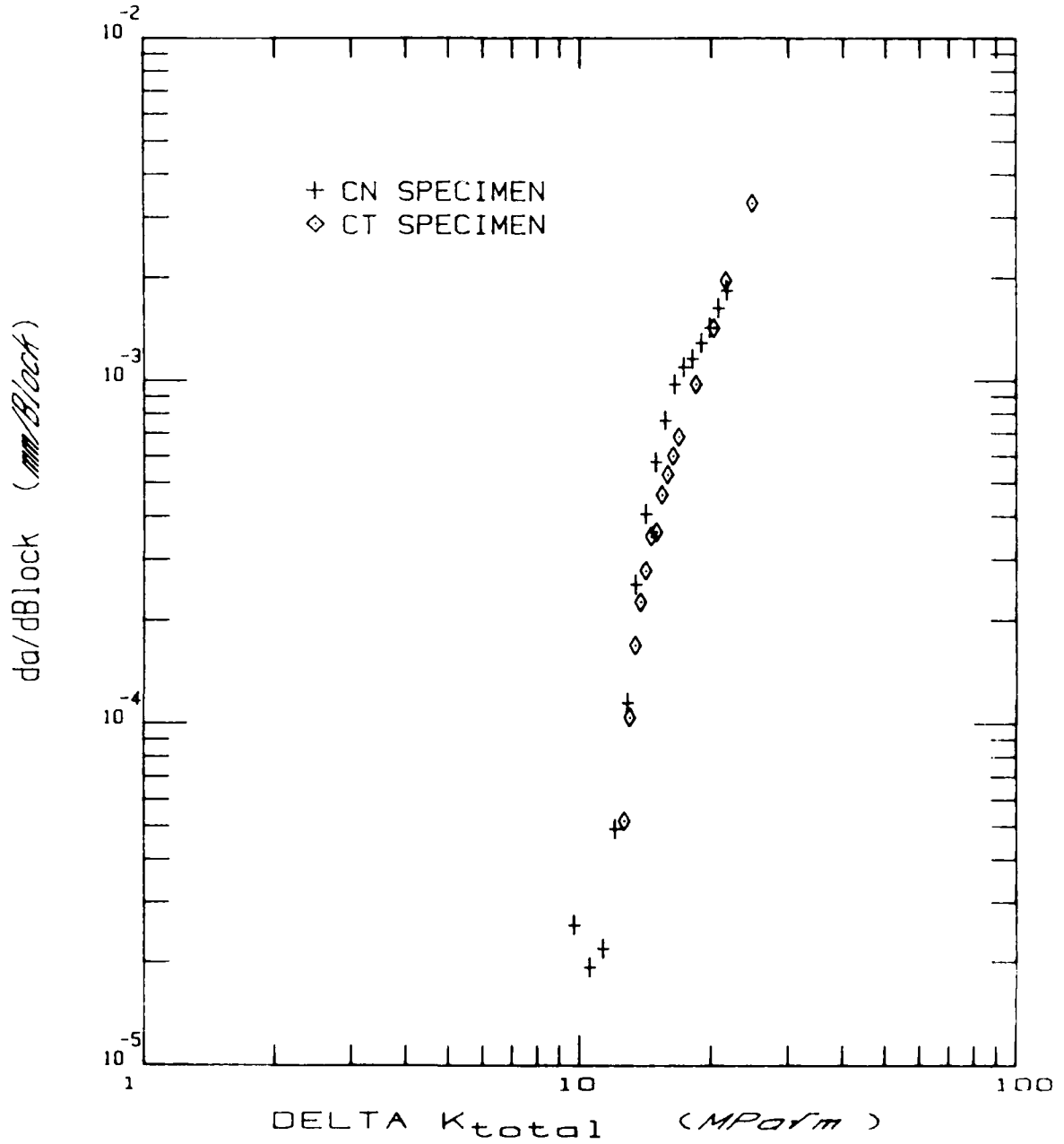

Fig. 13. Comparison of FCG rates in Ti-6Al-4V for CN and CT specimens at an amplitude ratio of 0.22 and a cycle ratio of 1000

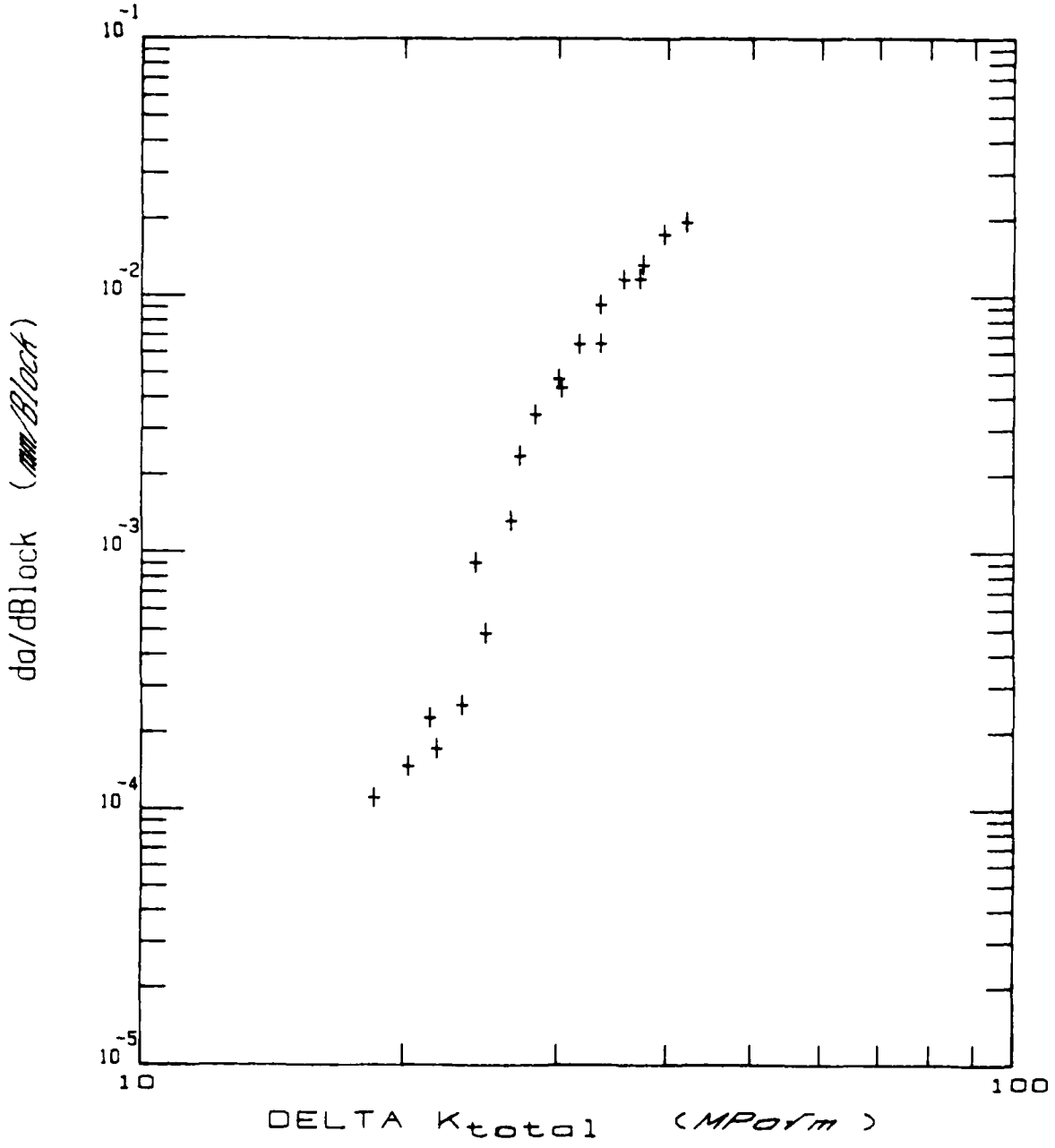

Fig. 14. FCG rates in CN specimens of Ti-5331S at an amplitude ratio of 0.12 and a cycle ratio of 10 000 (duplicate tests)

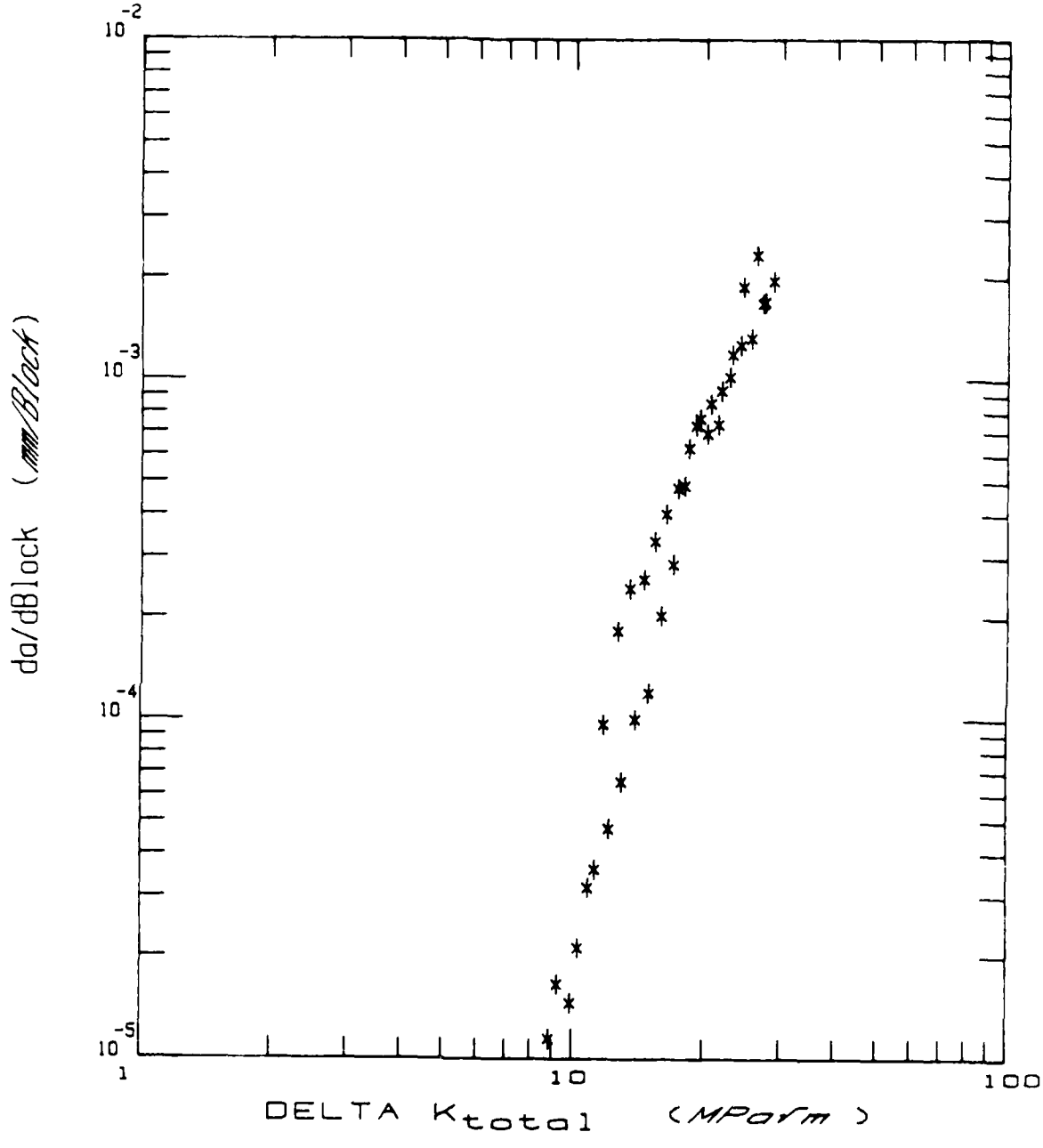

Fig. 15. FCG rates in CN specimens of Ti-5331S at an amplitude ratio of 0.22 and a cycle ratio of 1000 (duplicate tests)

chosen test conditions would give practical rates of FCG due to the overall major cycle when ΔK_{total} was less than ΔK_{onset}, whilst ensuring a marked change in growth rate following the onset of minor cycle crack growth. This proved not to be the case, as Figs. 16 and 17 indicate. Here the measured FCG rates are compared with those generated by major cycles alone. Unlike the results for Ti-6Al-4V, there is no agreement between the two sets of data at low stress intensity ranges, although as expected there is a subsequent divergence of the data at high stress intensity ranges. As a consequence an estimate of ΔK_{onset} cannot be obtained from such figures by taking ΔK_{onset} to be the value of ΔK_{total} intermediate between the greatest value of which the two sets of data agree and the lowest value at which they clearly diverge.

Table 4 reproduces the earlier results(2) for ΔK_{onset} values in Ti-5331S. It compares the values obtained by linear summation predictions, obtained from fatigue threshold data for the minor cycles, with the experimentally determined values for long through cracks in CT specimens. As a consequence, the data shown in Figs. 16 and 17 invite the question as to whether minor cycles can contribute to the overall FCG rates in CN specimens of Ti-5331S at levels of ΔK_{total} which are below levels of ΔK_{onset} established in CT specimens. Fig. 18 clearly shows that at higher stress intensity ranges, the FCG rates measured in CT and CN specimens at Q = 0.12 and n = 10 000 are essentially the same. In addition Fig. 19 shows the good correlation between the FCG rates in CN specimens tested at Q = 0.22 and n = 1 000 and the linear summation predictions based entirely upon CT data. Again this correlation is for stress intensity ranges in excess of the anticipated level of ΔK_{onset}.

TABLE 4 ΔK_{onset} values for Ti-5331S

Amplitude Ratio	ΔK_{onset} MPa$\sqrt{m}$	
	Predicted From Threshold Values	Experimental, CT Specimens
0.12	20.4	27.5 ± 2.4
0.12	20.4	22.6 ± 0.8
0.22	12.4	13.4 ± 0.7
0.22	12.4	13.2 ± 0.5

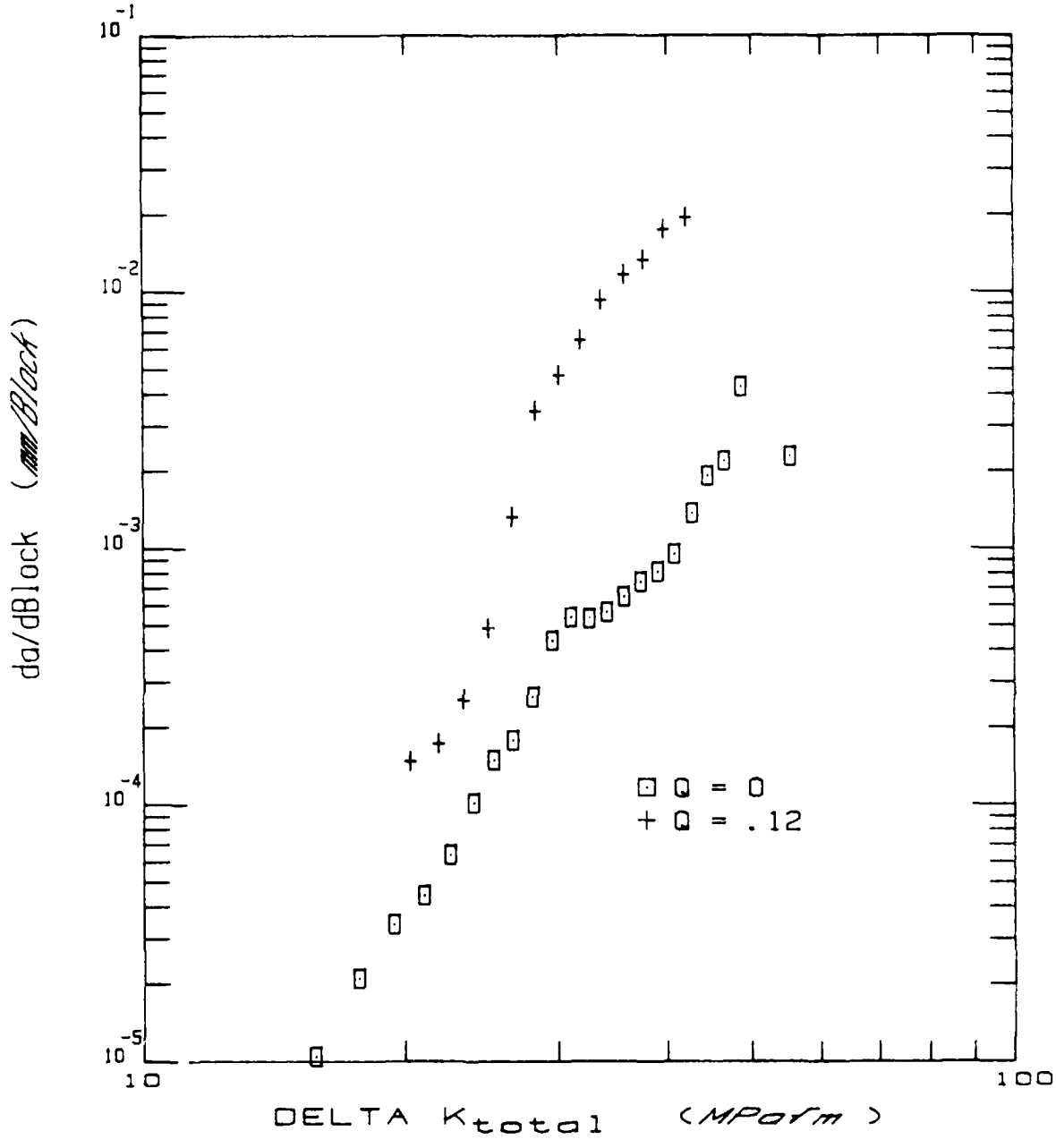

Fig. 16. Comparison of FCG rates for CN specimens of Ti-5331S for major cycles only (Q = 0) and combined major and minor stress cycles (Q = 0.12) and n = 10 000)

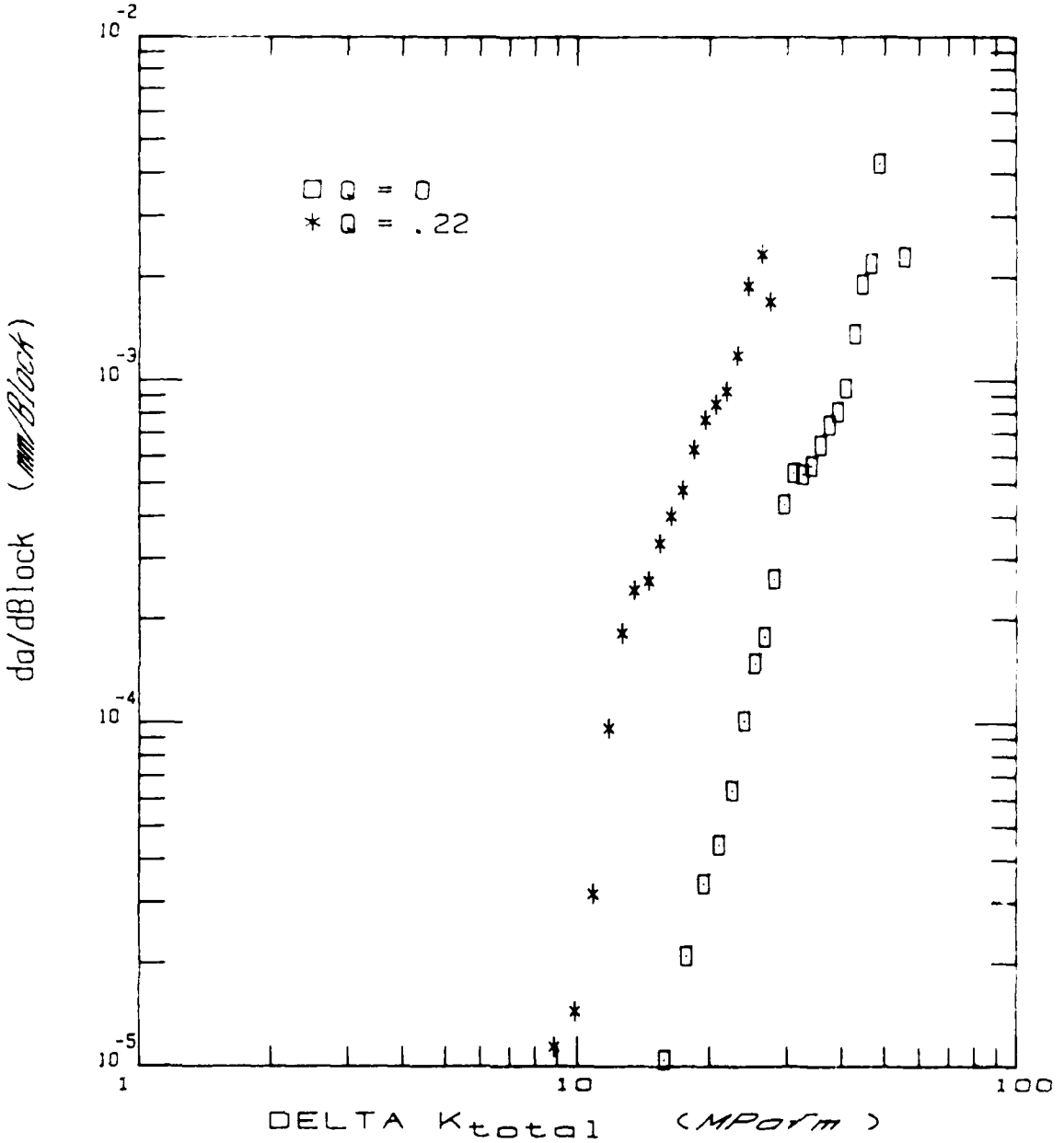

Fig. 17. Comparison of FCG rates for CN specimens of Ti-5331S for major cycles only (Q = 0) and combined major and minor stress cycles (Q = 0.22 and n = 1000)

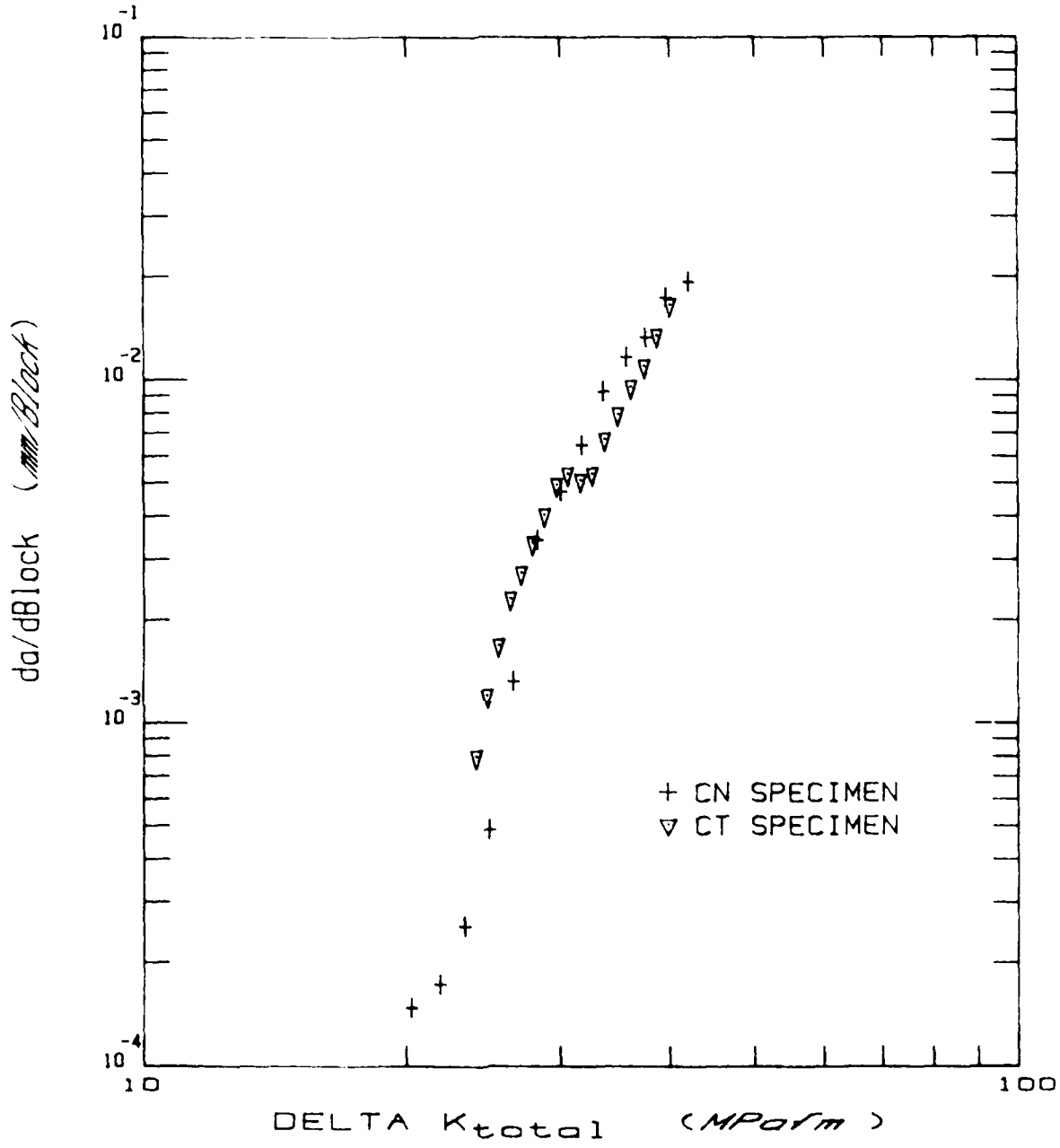

Fig. 18. Comparison of FCG rates in Ti-5331S for CN and CT specimens at an amplitude ratio of 0.12 and a cycle ratio of 10 000

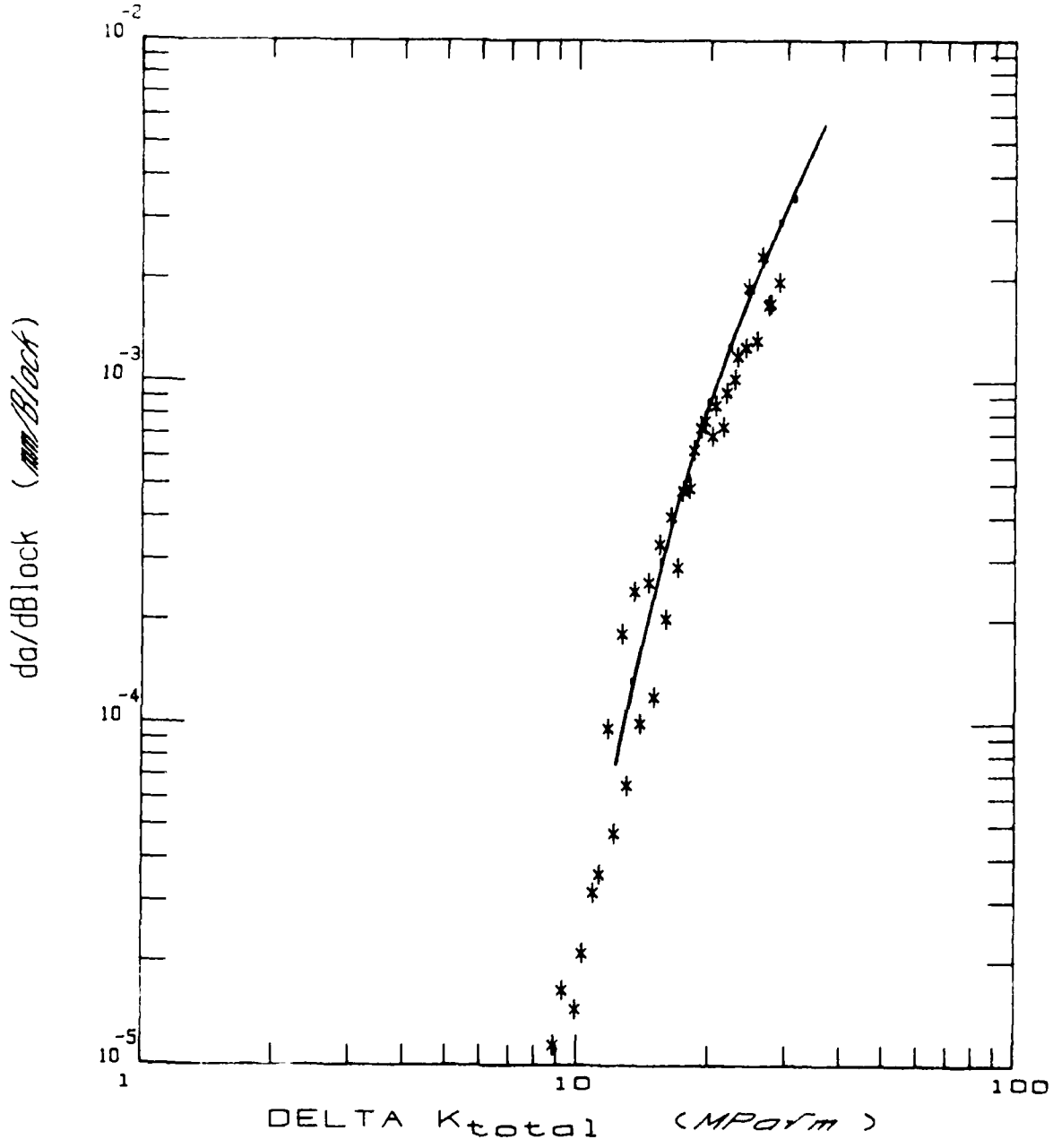

Fig. 19. Comparison of corner crack growth rates in Ti-5331S with the linear summation predictions based on CT data (full line). Test conditions of Q = 0.22, n = 1000 (duplicate tests)

SECTION 4

FRACTOGRAPHY

4.1 INTRODUCTION

Fractographic studies were made on six specimens which were representative of both test alloys and three loading conditions. These loadings are summarised in Table 5, together with the stress intensity ranges involved and the condition above which superimposed minor cycles could be expected to have some influence.

TABLE 5 Summary of test conditions for specimens examined fractographically

Specimen Number	Materials	Testing Loadings	ΔK_{total} (MPa$\sqrt{m}$)	ΔK_{onset} (MPa$\sqrt{m}$)
A1	Ti-6Al-4V	Major Cycles Only	15 - 55*	-
A3	Ti-6Al-4V	Major + Minor Cycles Q = 0.12 n = 10 000	16 - 50	19.0
A5	Ti-6Al-4V	Major + Minor Cycles Q = 0.22 n = 1000	10 - 26	11.7
B1	Ti-5331S	Major Cycles Only	19 - 65*	-
B3	Ti-5331S	Major + Minor Cycles Q = 0.12 n = 10 000	19 - 60	20.4+
B5	Ti-5331S	Major + Minor Cycles Q = 0.22 n = 1000	10 - 35	12.4+

* $\Delta K_{total} = \Delta K_{major}$

+ = Predicted Value

During the investigation, particular note was made of the occurrence of characteristic fracture mechanisms, namely: cyclic cleavage; striated growth including the development of block striation markings; and microvoid coalescence. In an earlier report, Powell and Henderson(2) described the fractographic features associated with these three cracking mechanisms for the two materials under test. Based upon their observations of the surface morphology of CT specimens,

they concluded that major cycle loadings produce a succession of largely faceted, striated, and dimpled fracture surfaces at progressively higher stress intensity ranges. In the case of combined major and minor stress cycles, the fracture surface topography prior to the onset of minor cycle crack growth is that given by major cycle loadings. Subsequently, the visible evidence of minor cycle activity is the development of 'block striations' which correspond to the periodic marking of the fracture surface by the major cycle loading, with the intervening crack advance resulting from the minor cycles of high stress ratio. The form of block striations in Ti-5331S, whilst on occasions similar to that in Ti-6Al-4V, generally differs in several respects. First, at a cycle ratio of 10 000, their occurrence is extensive and they grow to a spacing of 30 μm. Second, rather than being replaced by cyclic cleavage facets they are frequently superimposed on them. Third, those block striations having an appearance of brittle striations exhibit a greater spacing than ductile striations in immediately adjacent areas.

4.2 FRACTOGRAPHIC OBSERVATIONS FOR Ti-6Al-4V

The fractographic appearance of fatigue-induced cracks generated by the application of major cycles alone has been ascertained from a diagonal traverse of specimen A1 for stress intensity ranges between 15 and 55 MPa√m. Cyclic cleavage facets were present throughout this range but were dominant at the initial low stress intensity conditions. Fatigue striations were the principal feature observed with stress intensity ranges between 20 and 53 MPa√m. They were classical in form, being curvelinear and exhibiting some secondary branching and local variations in direction of FCG (Fig. 20). The striation width increased with the level of applied ΔK to a maximum of 2.5 μm. Naturally no feature resembling the block striations generated by the conjoint action of major and minor stress cycles was observed. At the highest levels of ΔK some microvoid coalescence was found.

By comparison, the fractographic features observed in the edge traverse of the same specimen displayed a marked reduction in the proportion of striated growth, which only became dominant at the higher stress intensities above 40 MPa√m, although first observed around 25 MPa√m. Less secondary cracking in the striations was apparent. There was an increase in cyclic cleavage to correspond with the reduction in striations. Microvoid coalescence was again observed at the highest stress intensity, while debris from relative movement of the metal under test was evident at low stress intensities.

Specimens A3 and A5 had previously been subjected to combined major and minor stress cycles at amplitude ratios of 0.12 and 0.22, and cycle ratios of 10 000 and 1000, respectively.

On specimen number A3, traversing diagonally across from the corner notch, cyclic cleavage facets were present at all ranges of ΔK_{total} examined (16 to 50 MPa√m) and they were the dominant morphological features (Fig. 21). No evidence of fatigue striations was

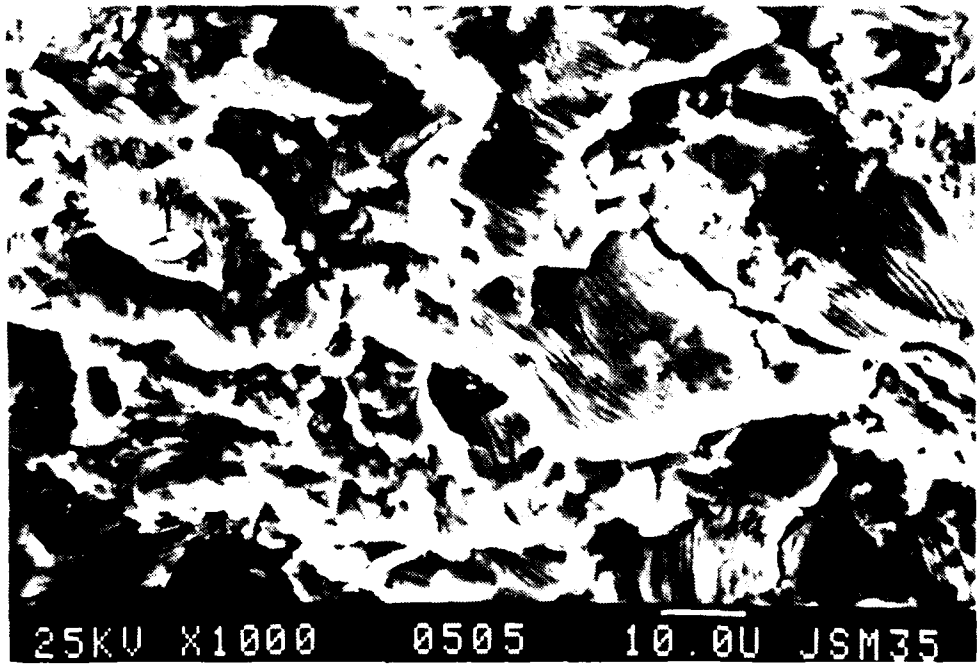

Fig. 20. Striated growth exhibiting wide variations in crack growth direction in Ti-6Al-4V. General crack growth direction from right to left. Test conditions: major cycles only. Stress intensity, ΔK = 34 MPa$\sqrt{m}$

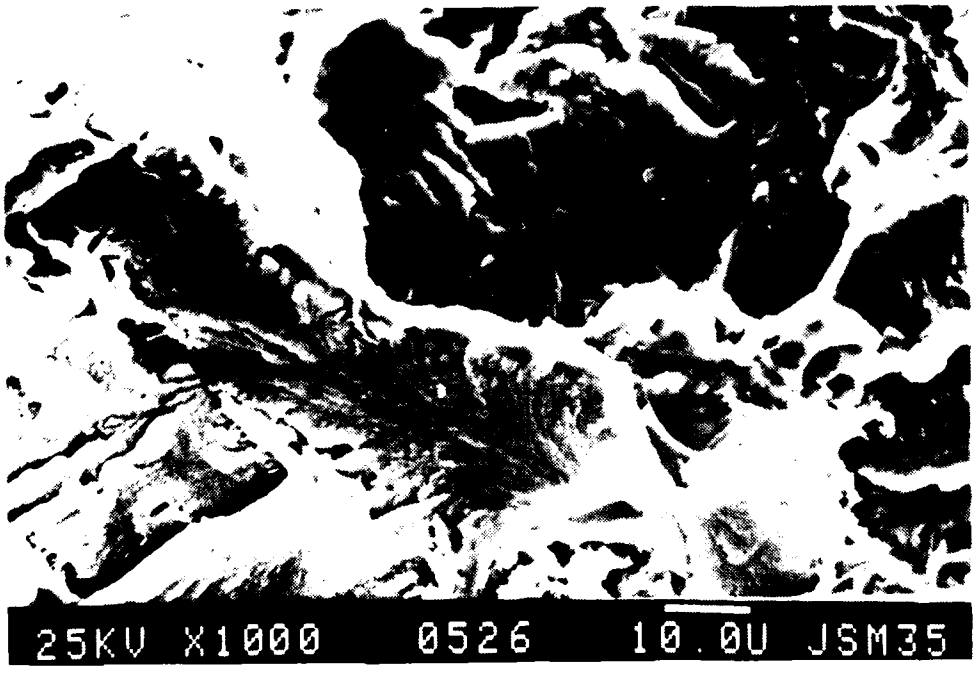

Fig. 21. Cyclic cleavage facets as the predominant surface morphology in Ti-6Al-4V. General crack growth direction from right to left. Test conditions: major + minor cycles, Q = 0.12, n = 10 000. Stress intensity, ΔK_{total} = 44 MPa$\sqrt{m}$

found, but there was evidence of microvoid coalescence at the highest stress intensity ranges.

When the specimen was examined along the edge, however, some evidence of the development of block striations was observed at crack lengths corresponding to values of ΔK_{onset} in the range 25 - 35 MPa√m. No microvoid coalescence was discernable.

Traversing diagonally across specimen A5, cyclic cleavage was observed at levels of ΔK_{total} between 10 and 25 MPa√m and was predominant except at the highest stress intensities. Block striations were only observed occasionally, being generally restricted to levels of ΔK_{total} of approximately 15 MPa√m; in addition they were superimposed upon cyclic cleavage facets which is unusual for Ti-6Al-4V (Fig. 22). Microvoid coalescence was absent.

By contrast, the fracture surface at the edge of the specimen contained a far greater proportion of block striations. They occurred on many small striation plateaux and displayed the usual characteristics of this fractographic feature (Fig. 23).

4.3 FRACTOGRAPHIC OBSERVATIONS FOR Ti-5331S

For Ti-5331S the following observations were made for the diagonal traverse across specimen B1 which had been tested solely under major cycles. Cyclic cleavage was observed at the lower stress intensity range, that is less than 40 MPa√m. Many of the facets were of large proportions with lengths of the order of 750 μm. Striated growth became apparent at a stress intensity range of approximately 35 MPa√m, and became the predominant surface feature at approximately 45 MPa√m. The striations were mostly of curvelinear form, with wide variations in their orientation in relation to the overall crack growth direction. The striation markings became very pronounced at the higher ranges of stress intensity, the distance between markings reaching 3.5 μm. There was some evidence of secondary cracking originating from the striations at all ranges of ΔK_{total} (Fig. 24). Microvoid coalescence was evident at the highest stress intensities, whilst at the lowest levels of ΔK_{total} debris from the fatiguing action was noted.

Along the edge of the same specimen cyclic cleavage was more prominent and a corresponding reduction in striated growth was observed. Microvoid coalescence occurred at the highest stress intensity range but no fretting debris was observed. Apart from the absence of debris, the variations in surface morphology between the diagonal and edge traverses is similar for both Ti-6Al-4V and Ti-5331S.

Specimens B3 and B5 were representative of tests using superimposed major and minor cycles. These tests again involved amplitude ratios of 0.12 and 0.22, and cycle ratios of 10 000 and 1000, respectively.

The results from a diagonal traverse of specimen B3 show that cyclic cleavage was observed at all stress intensity ranges between 19 and

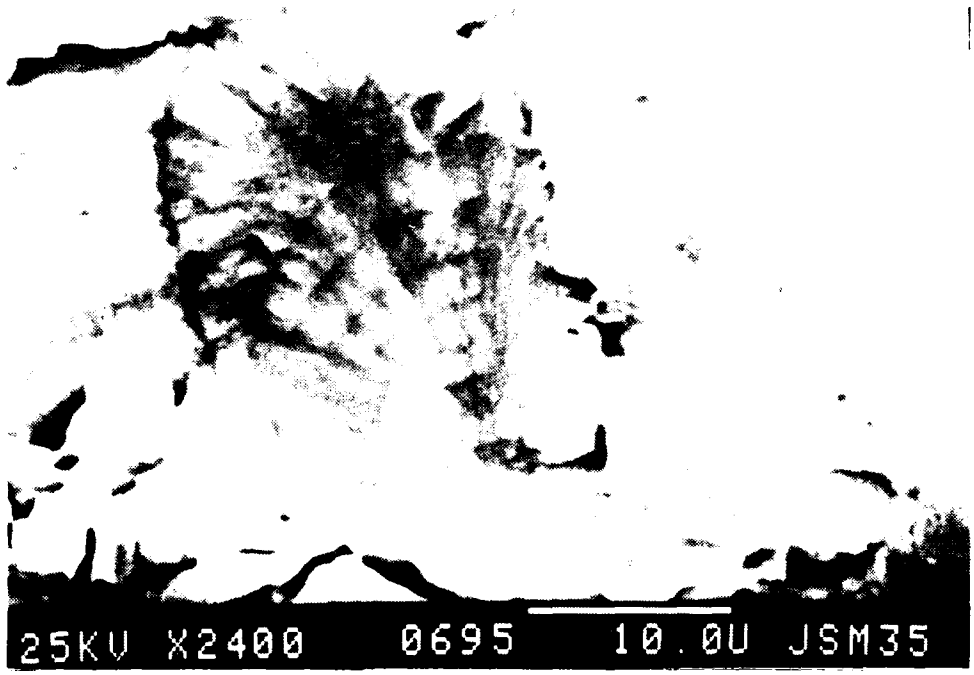

Fig. 22. Block striations superimposed upon cyclic cleavage facets in Ti-6Al-4V. General crack growth direction from right to left. Test conditions: major + minor cycles, Q = 0.22, n = 1000. Stress intensity, ΔK_{total} = 16 MPa√m

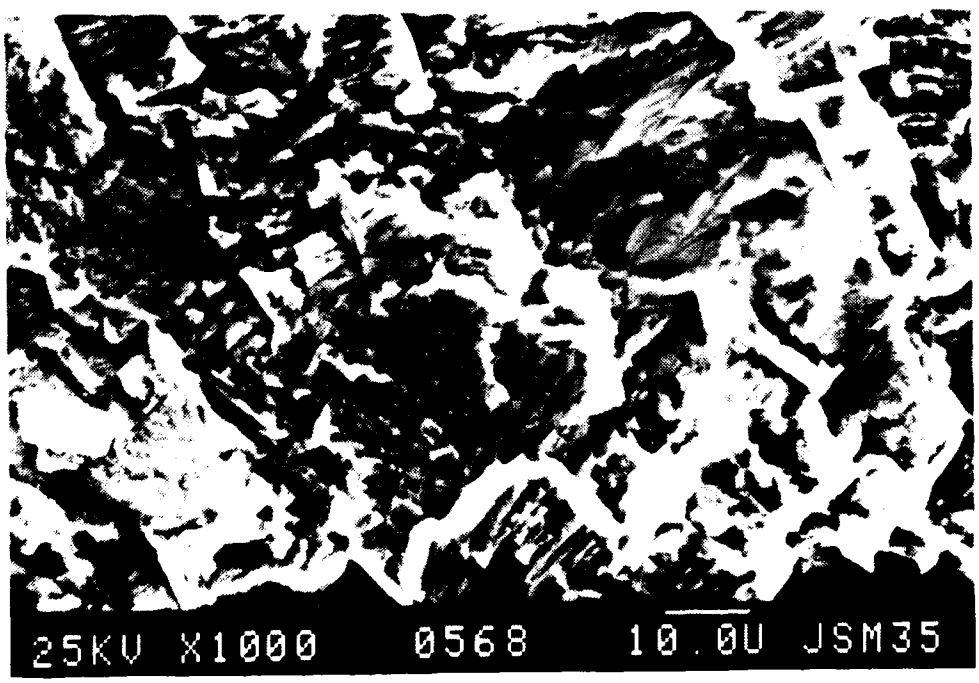

Fig. 23. Block striations on many small plateaux in Ti-6Al-4V. General crack growth direction from right to left. Test conditions: major + minor cycles, Q = 0.22, n = 1000. Stress intensity, ΔK_{total} = 26 MPa√m

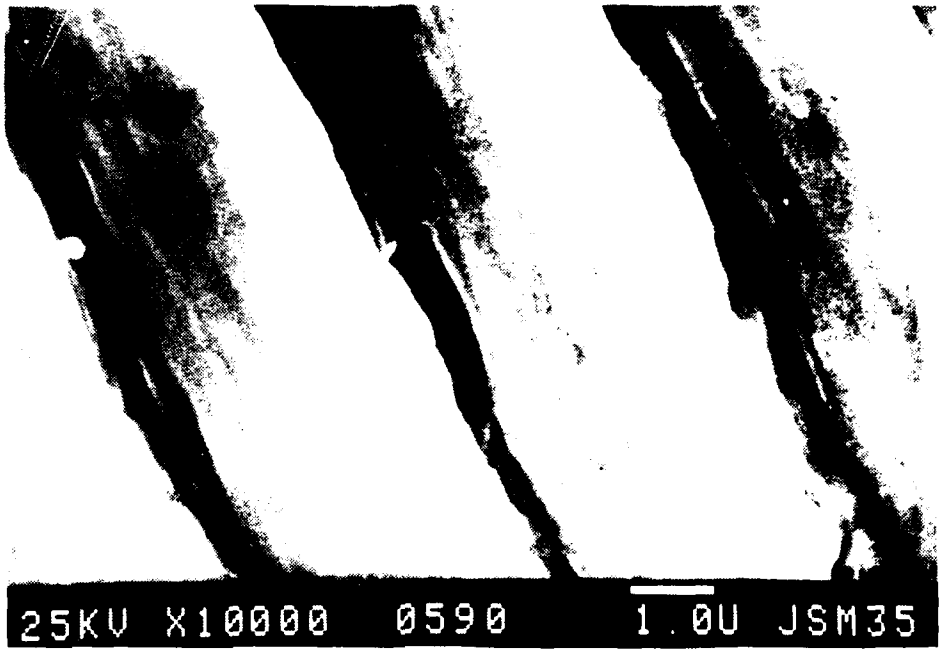

Fig. 24. Block striations in Ti-5331S with tendency for secondary cracking at striation markings. General crack growth direction from right to left. Test conditions: major cycles only. Stress intensity, ΔK = approx. 65 MPa$\sqrt{m}$

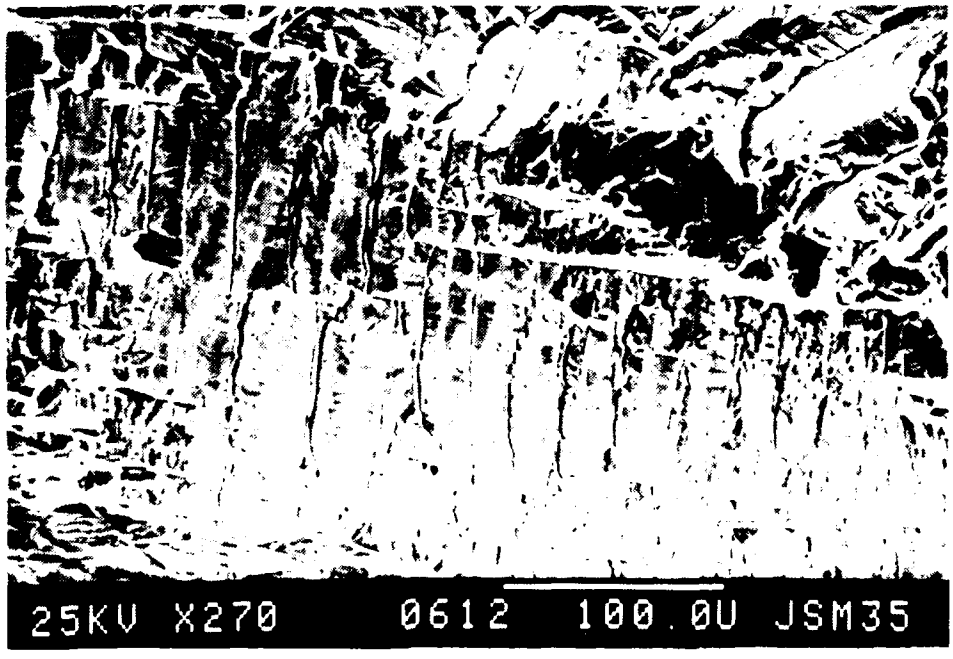

Fig. 25. Striations in Ti-5331S exhibiting sawtooth profile and deep secondary cracking. General crack growth direction from right to left. Test conditions: major + minor cycles, R = 0.12, n = 10 000. Stress intensity, ΔK_{total} = 53 MPa$\sqrt{m}$

60 MPa√m, and was dominant below 30 MPa√m. Above this level, block striations were clearly evident and they in turn became the dominant feature above 35 MPa√m. At the highest ranges of total stress intensity examined (50 - 60 MPa√m) the block striation width exceeded 20 μm. On occasions the block striations exhibited a sawtooth profile associated with deep secondary cracks (Fig. 25). At these high levels of ΔK_{total}, where striation markings were superimposed on cyclic cleavage facets, the striations took the form of troughs containing many small pores (Fig. 26), apart from this no form of dimpled fracture was to be seen. Also where the lattice planes within the grains were favourably oriented, it was possible to observe block striations which were continuous on regions of the fracture surface which were mutually perpendicular (Fig. 27).

Observations along the edge of the specimen were similar to the diagonal although cyclic cleavage was less evident and striated growth was more prominent. The block striations having a sawtooth profile were absent, but the presence of a dimpled structure within the striations superimposed on cyclic cleavage facets was again observed.

In a diagonal traverse across specimen B5, cyclic cleavage was observed particularly at low stress intensities with striated growth predominating above ΔK_{total} of 20 MPa√m. Block striation widths of 1.5 μm accompanied by a small amount of microvoid coalescence was associated with the final stages of this crack growth test which was terminated at a ΔK_{total} of 35 MPa√m. No significant difference in the fracture surface morphology of this specimen was found in the edge traverse.

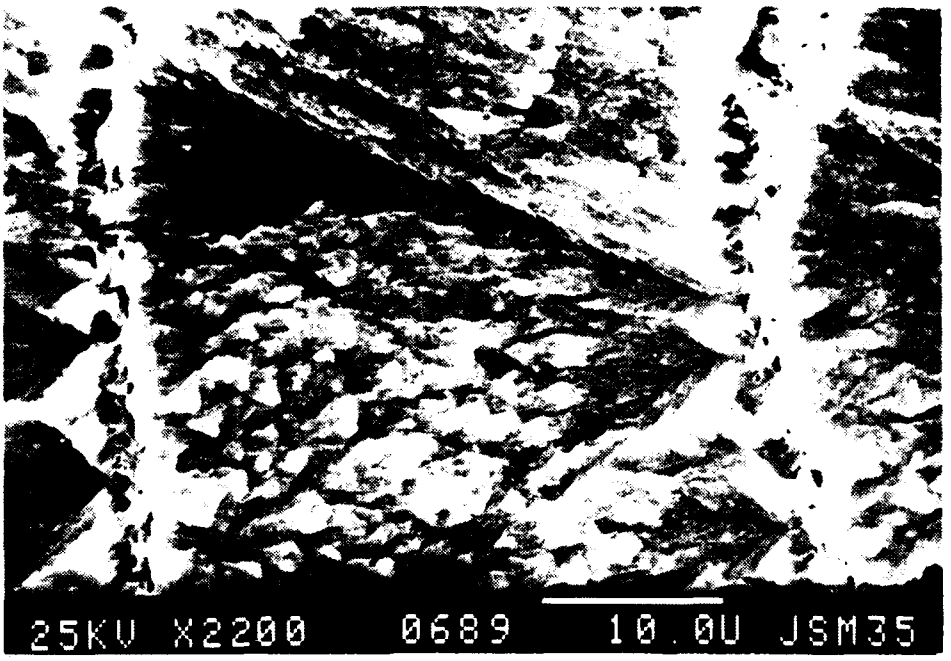

Fig. 26. Pores present within striation markings in Ti-5331S giving the appearance of microvoid coalescence. Local crack growth direction from right to left. Test conditions: major + minor cycles, Q = 0.12, n = 10 000. Stress intensity ΔK_{total} = 47 MPa√m

Fig. 27. Block striations on mutually perpendicular surfaces of Ti-5331S. Local crack growth direction from right to left. Test conditions: major + minor cycles, Q = 0.12, n = 10 000. Stress intensity, ΔK_{total} = 34 MPa√m

SECTION 5

FATIGUE CRACK GROWTH BEHAVIOUR IN GRAIN COARSENED Ti-5331S

Exploratory experiments have been conducted using CN test pieces of deliberately grain coarsened Ti-5331S, in order to emphasise the short crack growth regime and its possible effect upon the FCG rates under combined high and low cycle fatigue. Four fatigue loading sequences were applied in this series of tests, namely: major loading cycles only; minor loading cycles only; minor cycles superimposed upon major cycles at an amplitude ratio of 0.12; and minor cycles superimposed upon major cycles at an amplitude ratio of 0.22. Details of the loading conditions are given in Table 6.

TABLE 6 Fatigue test loading conditions

TEST NUMBER	MAJOR LOADS*		MINOR LOADS+		AMPLITUDE RATIO	CYCLE RATIO
	Maximum kN	Minimum kN	Amplitude ± kN	Mean kN		
C1	20.0	2	-	-	-	-
C2	-	-	1.8	18.2	-	-
C3	19.0	2	1.0	19.0	0.12	1000
C4	18.2	2	1.8	18.2	0.22	1000
C5	18.2	2	1.8	18.2	0.22	1000

* All major cycles of trapezoidal waveform at a frequency of 0.1 Hz.

+ All major cycles of sinusoidal waveform at a frequency of 150 Hz.

The first test piece subjected to major plus minor load cycles at an amplitude ratio of 0.22 produced an FCG rate which was very much greater than anticipated. The application of 1442 loading blocks, where one block is one major loading cycle with its associated superimposed minor cycles, caused the crack to grow nearly 3 mm. As a consequence little crack growth data were obtained from this test. When the test conditions involving separate minor cycles failed to propagate a short fatigue crack, the test piece was used to repeat the test an amplitude ratio of 0.22. Thus the sequence of experiments yielded FCG rates for microstructurally short crack subjected to loading conditions involving either separate major cycles or combined major and minor stress cycles.

In order to monitor the crack growth behaviour of each test piece,

the crack lengths, observed on the separate side faces were plotted against the number of elapsed major cycles (Fig. 28). Throughout this report, the terms left hand crack face and right hand crack face refer to the surfaces visible when the test piece is mounted in the testing machine and viewed on to the notch corner. As expected, the major cycles only test allowed the greatest number of loading cycles to elapse before termination. With increasing amplitude ratios, i.e., 0.12 and 0.22, the elapsed cycles to termination decreased, the first test at 0.22 most markedly so.

In a paper devoted to short FCG behaviour, Brown and Hicks(11) used a titanium alloy similar to Ti-5331S. In this study the relationship between FCG rate and stress intensity was investigated at a number of stress levels and modes of crack growth. Fig. 29 presents their findings for crystallographic crack growth. Also included by Brown and Hicks are data generated from a study of long crack growth in compact tension test pieces from the same material. Thus, the long crack near-threshold FCG rates are indicated by the solid line in Fig. 29. It should be noted that a different load ratio, 0.33 instead of zero, and a different test frequency, 100 Hz instead of 0.25 Hz, were used in the long crack testing. For the purpose of the present tests a further line, the broken line in Fig. 29, has been constructed. This line represents the fastest rate at which a short crack can be expected to propagate in the crystallographic mode and as such forms an upper bound to the data.

The FCG rates in grain coarsened Ti-5331S were first plotted against total stress intensity, ΔK_{total}, for each test piece; the two crack faces being treated separately. However, the mean crack length was also calculated to enable comparisons to be made with results from the previous tests on CN test pieces of Ti-5331S disc material. These previous tests used the DCPD method to measure crack length which produced an average crack length, based on a quarter circular crack in the test piece. FCG rates for the grain coarsened material and comparisons with the disc material are presented as Figs. 30 to 35. In each of these figures, the data from Brown and Hicks, corresponding to long crack near-threshold FCG rates at R = 0.33 have been inserted for the purpose of comparison.

It is evident from the results due to the application of major cycles only (Fig. 30) that there is a similarity in the FCG rates obtained from the left and right hand crack faces. All the results lie on or above the long crack reference data but are well below the short crack growth rate upper bound for the specifically crystallographic mode of crack growth. Fig. 31 compares the FCG rates observed in grain coarsened Ti-5331S and the disc grade of this alloy.

A short crack effect is again apparent in the results for grain coarsened material tested under combined major and minor stress cycles at an amplitude ratio of 0.12 (Fig. 32). Fig. 33 shows that below a ΔK_{total} of approximately 25 MPa$\sqrt{m}$ both the grain coarsened and the disc material show a common short crack effect. Subsequently, when the contribution to crack growth from the minor cycles becomes signi-

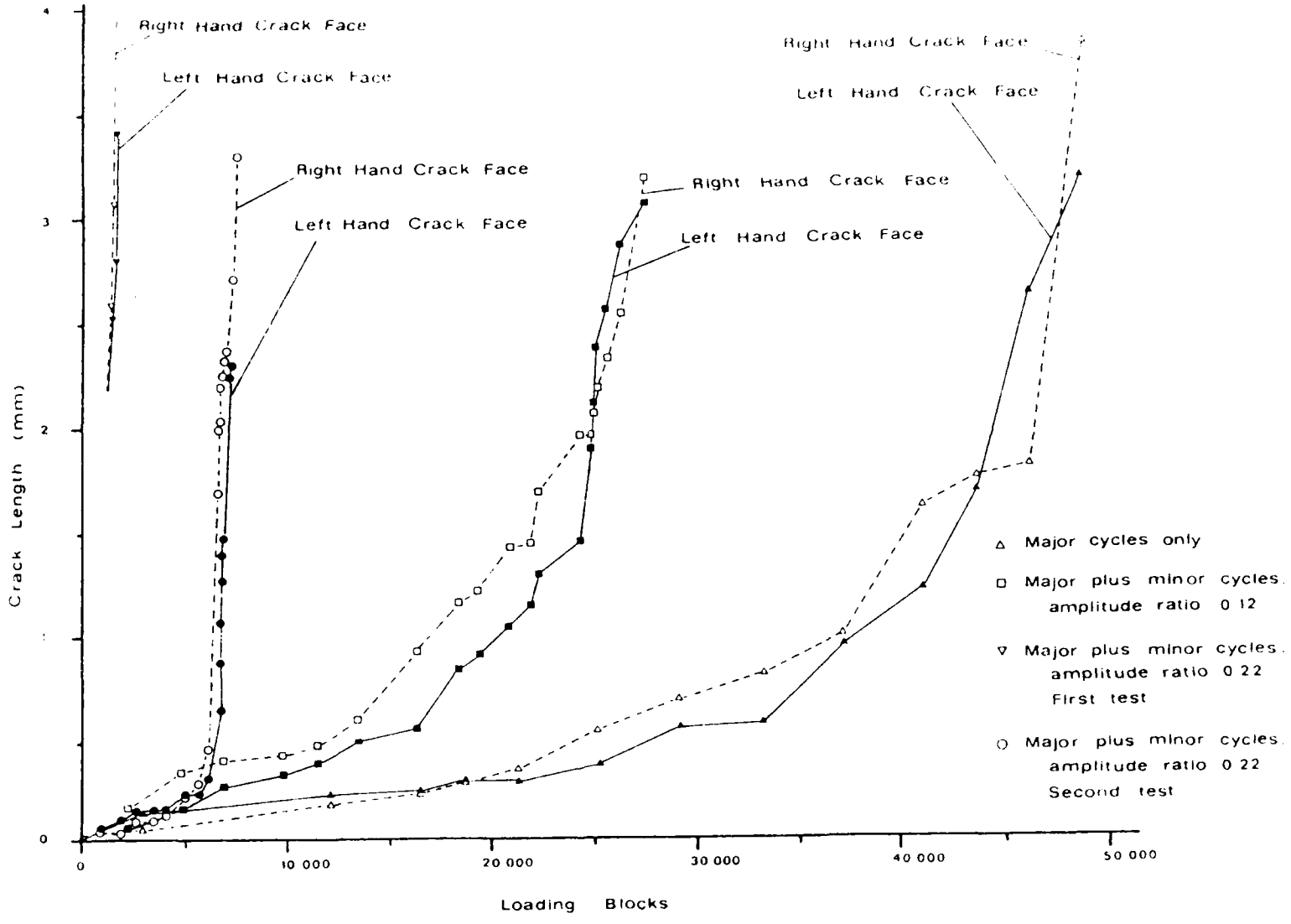

Fig. 28. Progress of the cracks through the test pieces of grain coarsened Ti-5331S

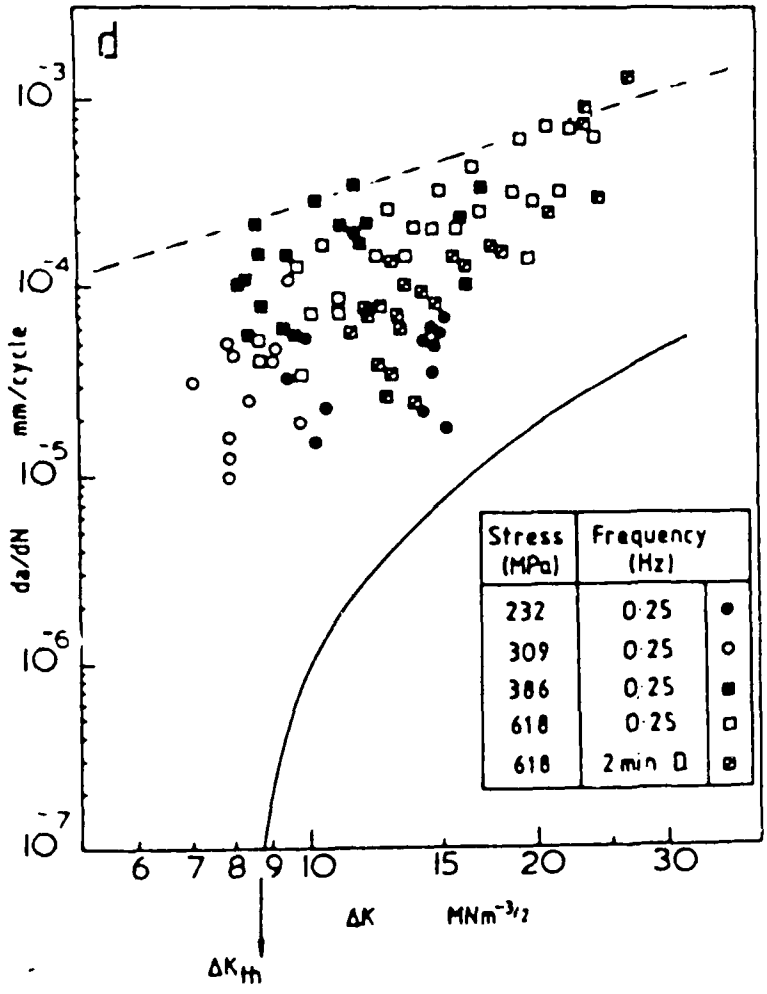

Fig. 29. FCG rates of short cracks in IMI 685 exhibiting a crystallographic mode of crack growth, compared to long crack data(11)

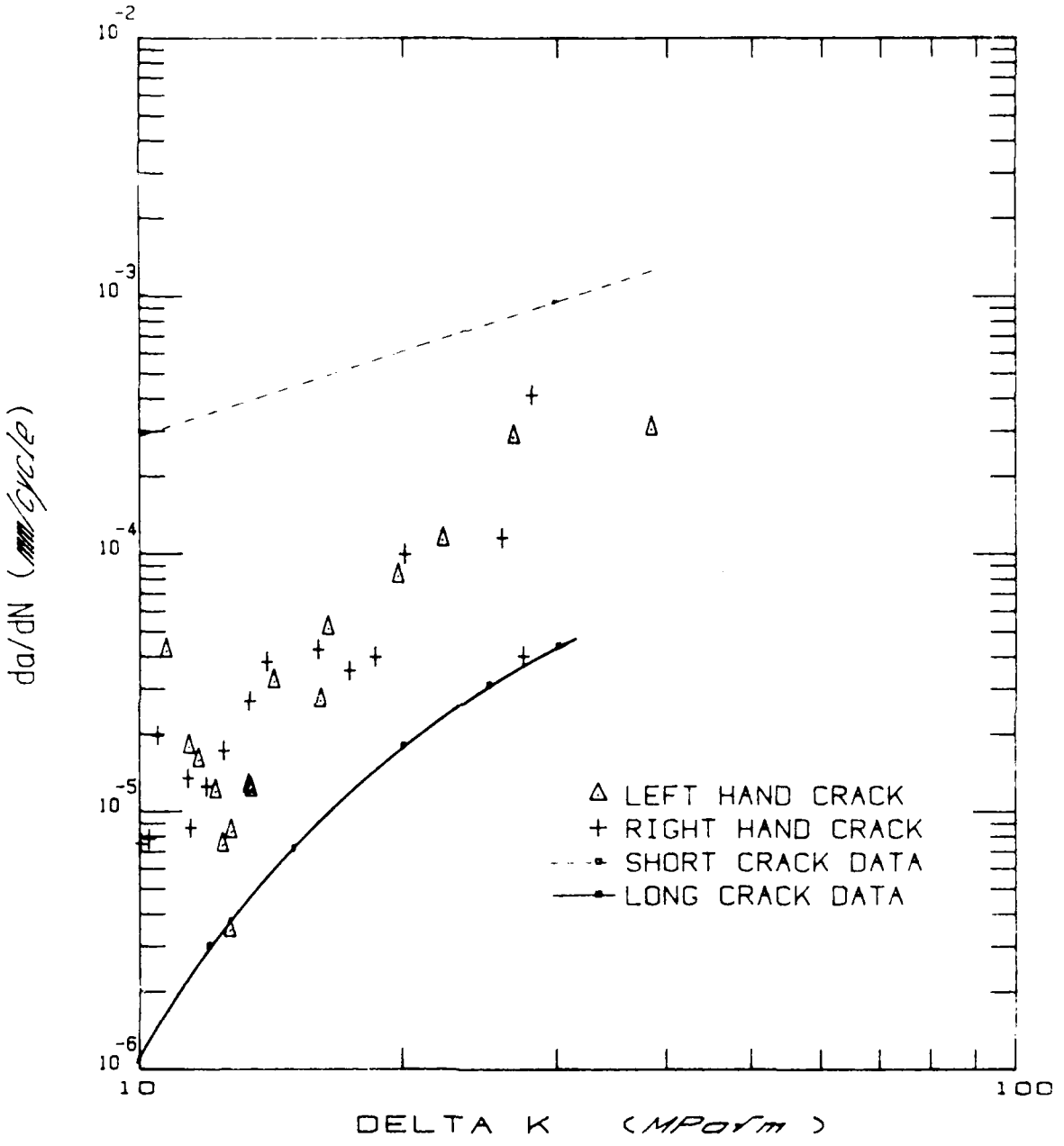

Fig. 30. FCG rates in grain coarsened Ti-5331S subjected to a major cycle loading

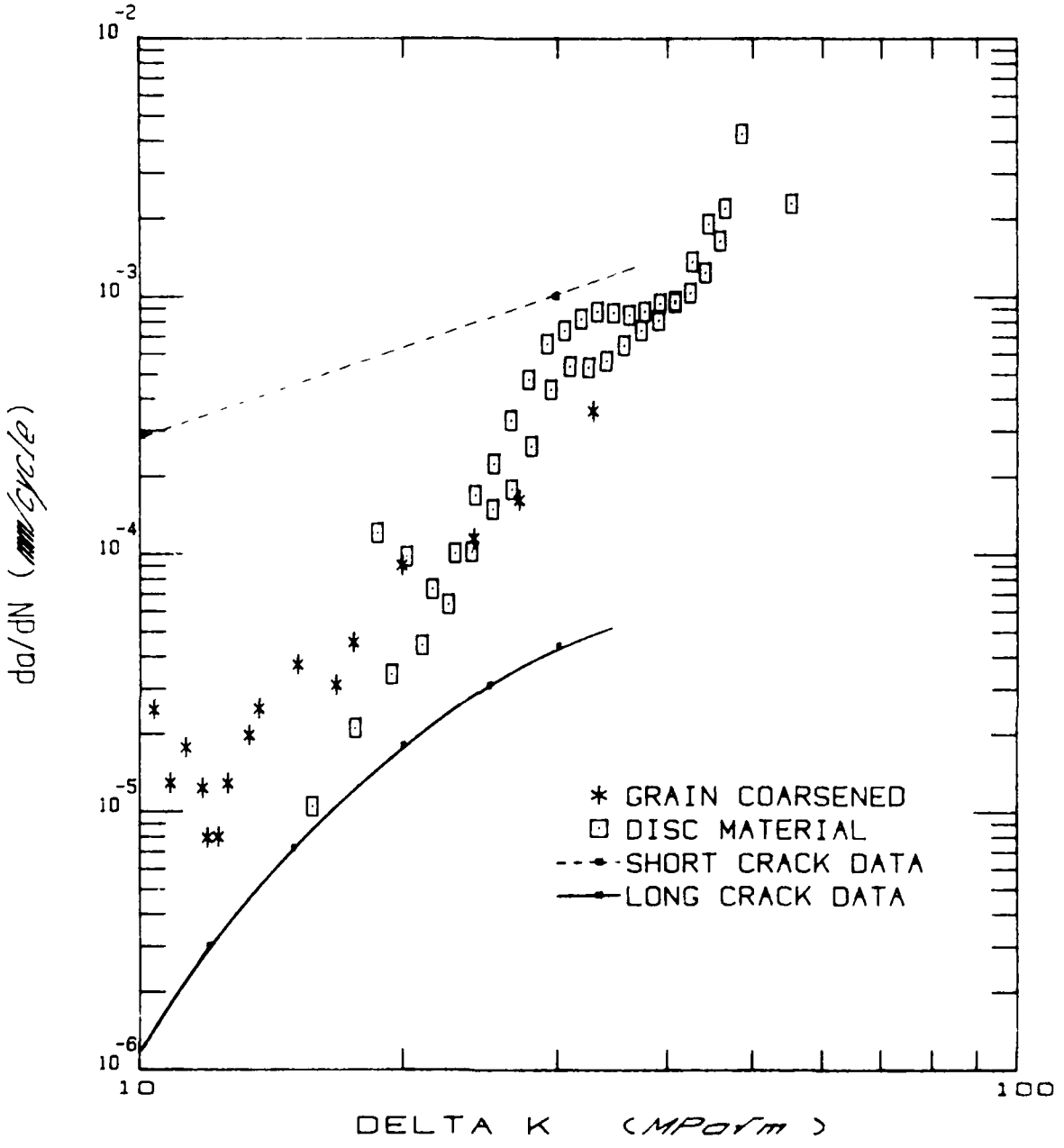

Fig. 31. Comparison of FCG rates in grain coarsened Ti-5331S and Ti-5331S disc material under a major cycle loading

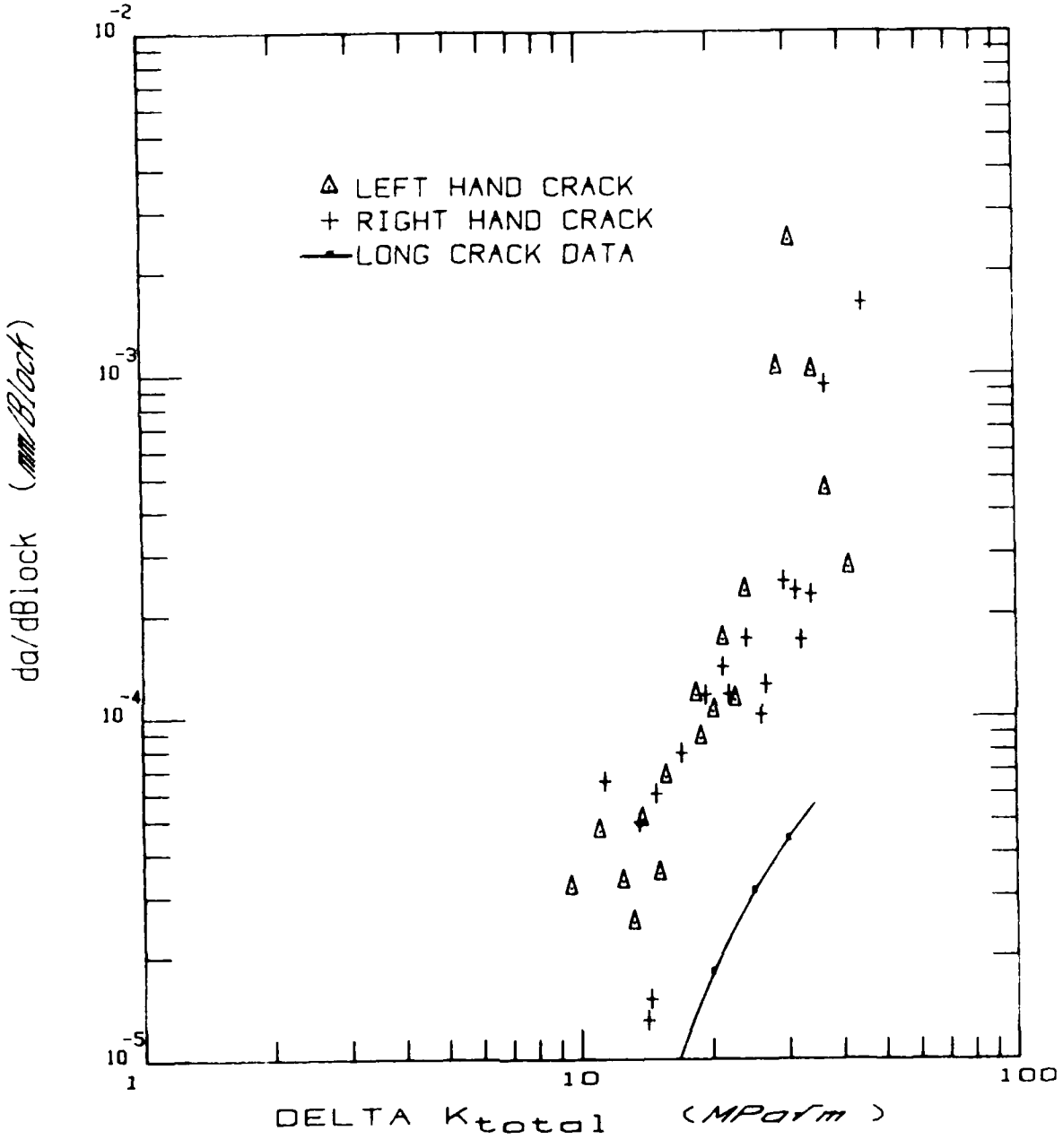

Fig. 32. FCG rates in grain coarsened Ti-5331S subjected to combined major and minor stress cycles at Q = 0.12 and n = 1000

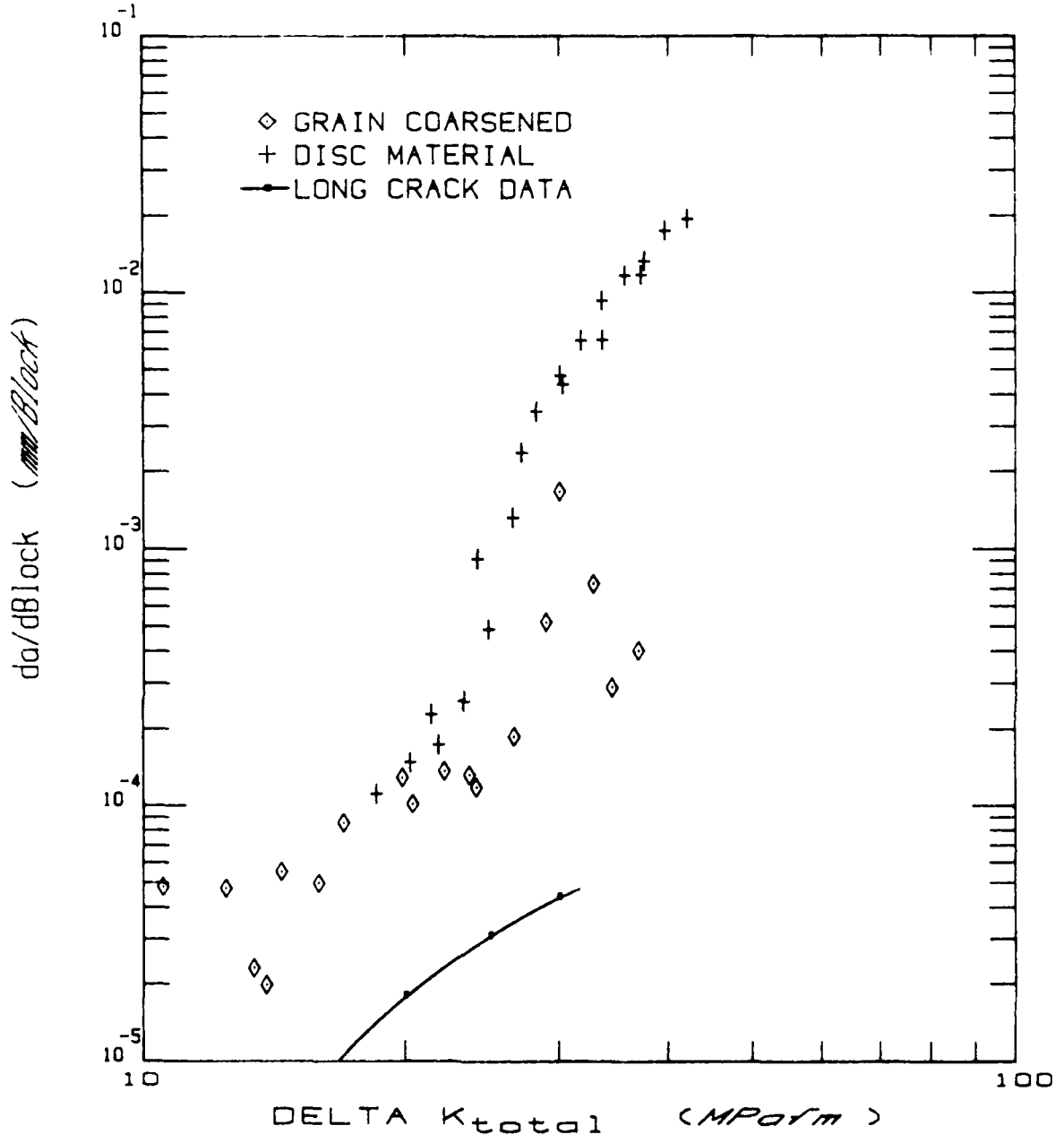

Fig. 33. Comparison of FCG rates in grain coarsened Ti-5331S and Ti-5331S disc material subjected to combined major and minor stress cycles at Q = 0.12

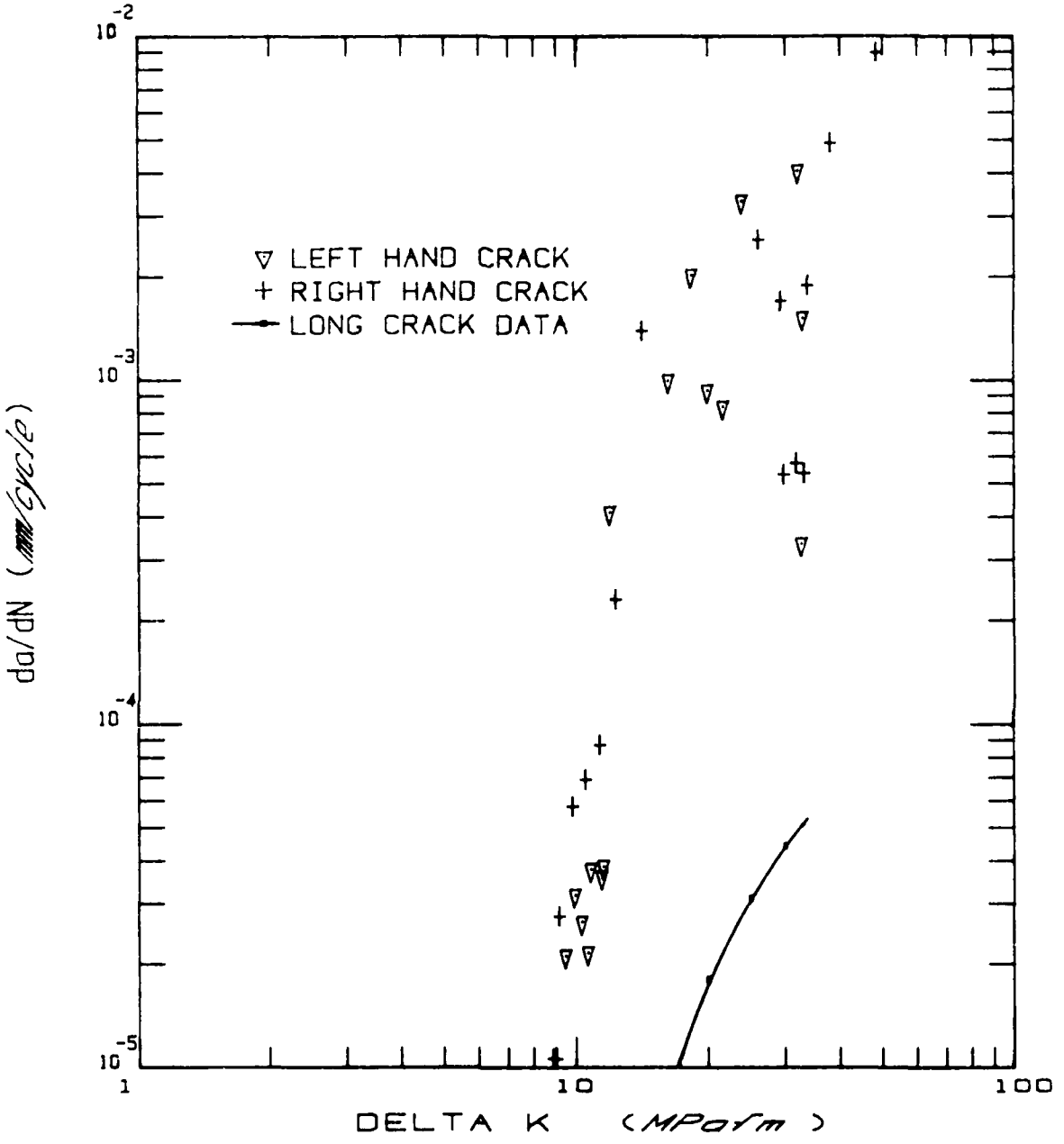

Fig. 34. FCG rates in grain coarsened Ti-5331S subjected to combined major and minor stress cycles at Q = 0.22 and n = 1000

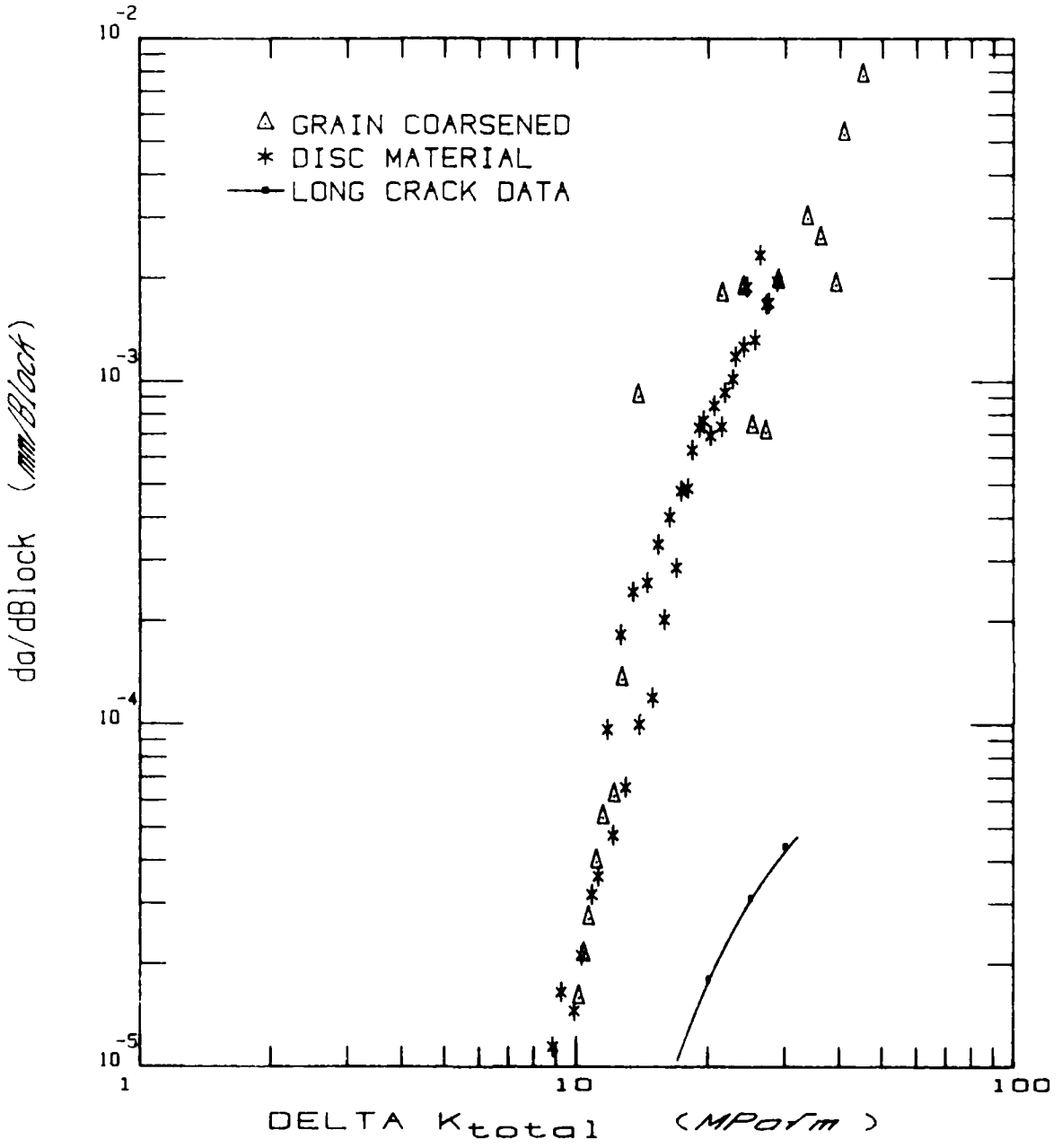

Fig. 35. Comparison of FCG rates in grain coarsened Ti-5331S and Ti-5331S disc material subjected to combined major and minor stress cycles at Q = 0.22 and n = 1000

ficant, the data for the two materials diverge, since a cycle ratio of 10 000 was used for the material whilst a cycle ratio of 1000 was applied to the grain coarsened material.

In the first test at an amplitude ratio of 0.22 the initial crack growth was so rapid that only a few results were obtained corresponding to the regime in which minor cycle damage was dominant. The results of a repeat test (Fig. 34) suggest the occurence of a short crack effect since growth rates of $2 - 6 \times 10^{-5}$ mm/block were observed at levels of ΔK_{total} below the ΔK_{onset} value of 12.4 MPa$\sqrt{m}$ predicted from long crack threshold data. However, the growth rates rise rapidly as ΔK_{total} increases and the effect on growth rate of the minor cycles becomes dominant. Fig. 35 shows the comparison with FCG rates measured for the disc material. There is a good correlation at the lower stress intensity ranges, whilst at the higher ranges there is greater scatter but this is about the mean of the data for the disc material.

SECTION 6

DISCUSSION

6.1 FATIGUE CRACK GROWTH MECHANISMS

The morphology of fatigue-induced crack surfaces revealed in diagonal traverses of CN type test pieces have been compared with the observations from centre line traverses of CT type test pieces tested under the same loading conditions. As the level of ΔK increased similar changes in morphology were seen, which is as expected, since, in general, similar FCG rates were measured from the two test piece designs. When the crack growth rates in Ti-5331S subjected to combined major and minor stress cycles were retarded relative to the linear summation predictions, it was evident from the fracture surfaces of both specimen types that this effect arose, at least in part, from an interference to the mechanisms of minor cycle crack growth. This interference is caused by the periodic marking of the fracture surface with fatigue striations generated in response to the major cycle loading. The fractographic observation of the regeneration of tear ridges at the major cycle striation markings (Fig. 27) indicated an effective lengthening of the crack front which would produce a reduction in the crack growth rate.

Previously, and on the basis of the fractographic examination of CT specimens, it had been suggested(2) that in Ti-6Al-4V striated growth and cyclic cleavage were mutually exclusive. Now, in CN specimens subjected to combined major and minor stress cycles at an amplitude ratio of 0.22 and a cycle ratio of 1000, block striations superimposed on cyclic cleavage facets have been observed. This is not considered to be an effect of specimen design, as such, rather a consequence of the specimen orientation involved. The CT test pieces were cut so that the fatigue crack plane coincided with the radial/axial plane of the original disc, i.e., the approximate orientation of the fir tree roots; whilst of necessity the cutting of the longer CN specimens from a fan disc required that their fatigue crack plane was axial/tangential. Texture measurements have shown that preferred orientations exist within such discs(12). Basal planes lie within a few degrees of the radial/axial plane with an intensity of the order of four times random, whilst axial/tangential textures are weak and may indeed be absent.

Using the technique of electron channelling patterns, Ward-Close and Beevers(13) have shown that the fracture mode in α titanium is dependent upon the orientation of each grain relative to the maximum tensile loading axis. Cyclic cleavage occurs on the (0002) basal plane when the basal pole lies within 60° of the tensile axis, the incidence of cleavage fracture depending on the level of stress intensity range and evironment. Striations are, by contrast, formed on planes normal to the (0002) basal plane with the striation front parallel to the [0001] crystal direction. Striations will form where the c-axis of a close packed hexagonal unit cell is more than 75° from

the tensile axis and more than 50° from the macroscopic FCG direction. These observations, which may be summarised in a grain orientation control map(13), show that in α titanium cyclic cleavage and striated growth are mutually exclusive.

The previous failure to observe block striations on cleavage facets of Ti-6Al-4V may, therefore, have arisen from the inspection of a crack growth plane which coincided with the maximum intensity of basal planes, which were suitably orientated for cyclic clearage but inconveniently orientated for striated growth. The subsequent examination of the axial/tangential plane, which presents a more random distribution of crystal planes relative to the macroscopic plane of cracking, has however shown that occasionally the two forms of growth can occur in combination. As a consequence block striation markings superimposed on cyclic cleavage facets have now been observed in Ti-6Al-4V, Ti-5331S and RR58 high strength aluminium alloy(14), occurring occasionally in Ti-6Al-4V and RR58, and frequently in Ti-5331S.

Brown and Hicks report(10) that the edge region of CN type specimens in nickel-based superalloys displayed a marked difference in fracture surface morphology in comparison with the centre. No similar effect was observed in either titanium-based alloy tested at room temperature. However, some differences between the centre and edge regions have been found in the titanium alloys when examined at higher magnification than the x50 employed by Brown and Hicks. In particular the amount of striated crack growth was seen to vary. Where major stress cycles alone were applied, both Ti-6Al-4V and Ti-5331S contained fewer striations in the edge regions. Brown and Hicks suggest that the greater proportion of plane stress to plane strain in CT relative to CN specimens gave rise to the FCG rate discrepancies observed in these nickel-based alloys at stress intensity levels greater than 20 MPa$\sqrt{m}$. With respect to FCG rates in CN specimens, they also considered that 'should the plane stress growth occur by a significantly different mechanism to that of the bulk of the test piece, then the degree of retardation produced could be further enhanced'. The results presented here indicate that the same discrepancy in major cycle FCG rates is exhibited in Ti-6Al-4V, but not in Ti-5331S. Consequently, the similar variations in FCG mechanism between the edge and bulk of the specimens observed for the two materials cannot account for the observed differences in crack growth behaviour displayed between the two test piece designs.

Under combined loading, the FCG rates observed in CT and CN specimens coincided. A fractographic traverse of the edge region of CN specimens subjected to this type of loading generally revealed a greater proportion of striated growth when compared to a diagonal traverse. Thus depending on the form of the loadings, either a greater or lesser proportion of striated growth can occur in Ti-5331S, yet identical FCG rates are observed in both CT and CN specimens. Again the indications are that differences in the crack growth mechanism cannot be the cause of the presence or absence of discrepancies in the FCG rate.

What then is a plausible explanation for the absence or presence of discrepancies in the FCG rate between specimen designs? When a CT type specimen of Ti-6Al-4V was subjected to major stress cycles alone, measurement of crack closure has shown(2) that the stress intensity associated with crack opening was initially low but tended to rise with applied ΔK, which is consistent with a plasticity-induced property. As a consequence of the greater proportion of plane stress within CN specimens, plastically-induced crack closure would be enhanced. This would account for the crack growth retardation observed for this type of specimen. Results from many measurements of crack closure in Ti-5331S with CT specimens has demonstrated that a high level of surface roughness induced crack closure is present, being a direct consequence of the microstructure of the material. Any additional type of closure caused by plasticity within the material would be small by comparison and it is reasonable to expect that CN and CT test pieces would display similar effects on FCG rates. Applying major and minor stress cycles, the crack growth becomes largely closure free, thus the same crack growth rates would be expected in both CT and CN specimens, and it is found to be so.

Table 7 summarises pertinent details highlighting the single instance where FCG rate measurements from CN specimens were retarded with respect to those from CT specimens. This corresponds to the sole condition in which a variation in the ratio of plane stress to plane strain would be expected to have a significant influence.

TABLE 7 Comparison of crack growth rate, fracture mechanisms and closure behaviour as a function of test loading conditions

Loading Conditions	FCG Rate, CN Relative to CT Specimens	Striated Growth Proportion Edge to Diagonal	Crack Closure Behaviour in CT Specimens
	Ti-6Al-4V		
Major cycles only	Less	Less	Low, plasticity-induced. Affected by proportion of plane stress to plane stain
Major + minor cycles Q = 0.12 n = 10 000	Same	More	Largely absent
Major + minor cycles Q = 0.22 n = 1000	Same	More	Largely absent

TABLE 7 (CONCLUDED)

Loading Conditions	FCG Rate, CN Relative to CT Specimens	Striated Growth Proportion Edge to Diagonal	Crack Closure Behaviour in CT Specimens
	Ti-5331S		
Major cycles only	Same	Less	High, surface - roughness induced
Major + minor cycles Q = 0.12 n = 10 000	Same	More	Largely absent
Major + minor cycles Q = 0.22 n = 1000	Same	Similar	Largely absent

6.2 CRACK GROWTH LIFE PREDICTIONS

In those materials, such as Ti-6Al-4V, in which different FCG rates are observed in CT and CN specimens subjected to major cycles only, the fatigue crack propagation lives associated with flaws in aero-engine discs are more accurately predicted using the crack growth data from CN specimens, as Pickard et al(9) have shown. When damaging minor cycles are present in substantial numbers their contribution to the overall growth is dominant. In these circumstances differences between the FCG rates for major cycle loadings at $\Delta K \geq 20$ MPa$\sqrt{m}$ become unimportant. This is the reason why the results from CN and CT specimens of Ti-6Al-4V subjected to combined low and high cycle fatigue, together with the linear summation predictions, can be in total accord. This agreement is encouraging since published FCG and fatigue threshold data are generally for CT specimens and single frequency loadings; yet it would appear reasonable to apply such data, using the linear summation rule, to the growth of corner cracks in highly stressed regions of critical rotating aero-engine components. It should be noted that the agreement has been established for room temperature where time dependent processes are often small. At the maximum operating temperature of the material the two specimen designs may show a different response due to time dependent processes by virtue of the differing stress levels required to produce the same ΔK within them. This represents an important area for future research.

The FCG behaviour of Ti-5331S contrasts with that of Ti-6Al-4V in several ways. For example, the high level of roughness-induced crack closure present in Ti-5331S results in FCG rates for a major cycle

loading which are significantly slower than those prevailing in Ti-6Al-4V. Under combined major-minor cycle loadings possessing high cycle ratios, the extent of the useful life of a component is effectively limited by the onset of minor cycle crack growth. The similar fatigue threshold values, at a high tensile mean stress, show that the resistance of Ti-5331S to minor cycle FCG is only marginally greater than that of Ti-6Al-4V(2). Thus it is that Ti-5331S might be expected to show greater crack propagation lives under combined major and minor cycle loadings. This is not because of a significant delay in minor cycle crack growth, nor subsequent retardations in FCG rates, but rather because of its apparently slower major cycle crack growth rates prior to reaching the ΔK_{onset} conditions.

The foregoing argument indicates that Ti-5331S is to be preferred where a lifing policy of retirement for cause is adopted; but the test results from CN specimens now suggest that the supposed superiority of Ti-5331S may not be realised. The level of ΔK_{onset} for this material could not be determined experimentally from the CN test results, since the FCG data for loadings of major cycles only, and combined major and minor stress cycles, did not appear to merge at the lowest ranges of stress intensity. An important feature of the FCG behaviour of Ti-5331S is the occurrence of enhanced crack growth rates at crack lengths which are similar to the grain size of the material. Fig. 36 summarises the limited experimental data relating to this effect. It shows that the FCG rates for a major cycle loading may deviate at the lowest ranges of stress intensity, the growth rates for relatively short cracks in CN specimens in both disc and grain coarsened material being represented by a scatter band which extends above the FCG rate curve for long cracks in Ti specimens. Fig. 36 also shows the FCG rate curve for a loading of combined major and minor stress cycles at Q = 0.12 and n = 10 000. It is now seen that the initial part of this curve, for ΔK_{total} less than the predicted level of ΔK_{onset}, lies close to the scatter band for microstructually short crack growth under a major cycle only loading. In practice, therefore, quarter circular cracks in aeroengine discs of Ti-5331S subjected to combined major and minor stress cycles, could initially display rapid growth rates due to short crack effects, until the crack size was sufficient for the minor cycles to give even faster growth rates, leading to early fracture. In this case, the fatigue crack propagation life predictions based solely upon the integration of long (CT) crack growth data would be inherently unsafe.

The very short fatigue crack propagation lives which can result from the superimposition of vibratory stresses of large amplitude are clearly indicated by the two test results on grain coarsened material at Q = 0.22 (Fig. 29). The very rapid crack growth of the first test is readily apparent, and the most likely explanation of this rapid growth is that the enlarged grains through which the crack grew initially were of such an orientation that very favourable planes were presented for crack propagation relative to the direction of loading. It is clear that the minor cycles had been active in their contribution to overall crack growth early in the test and this raises the possibility that, due to short crack effects, they become active

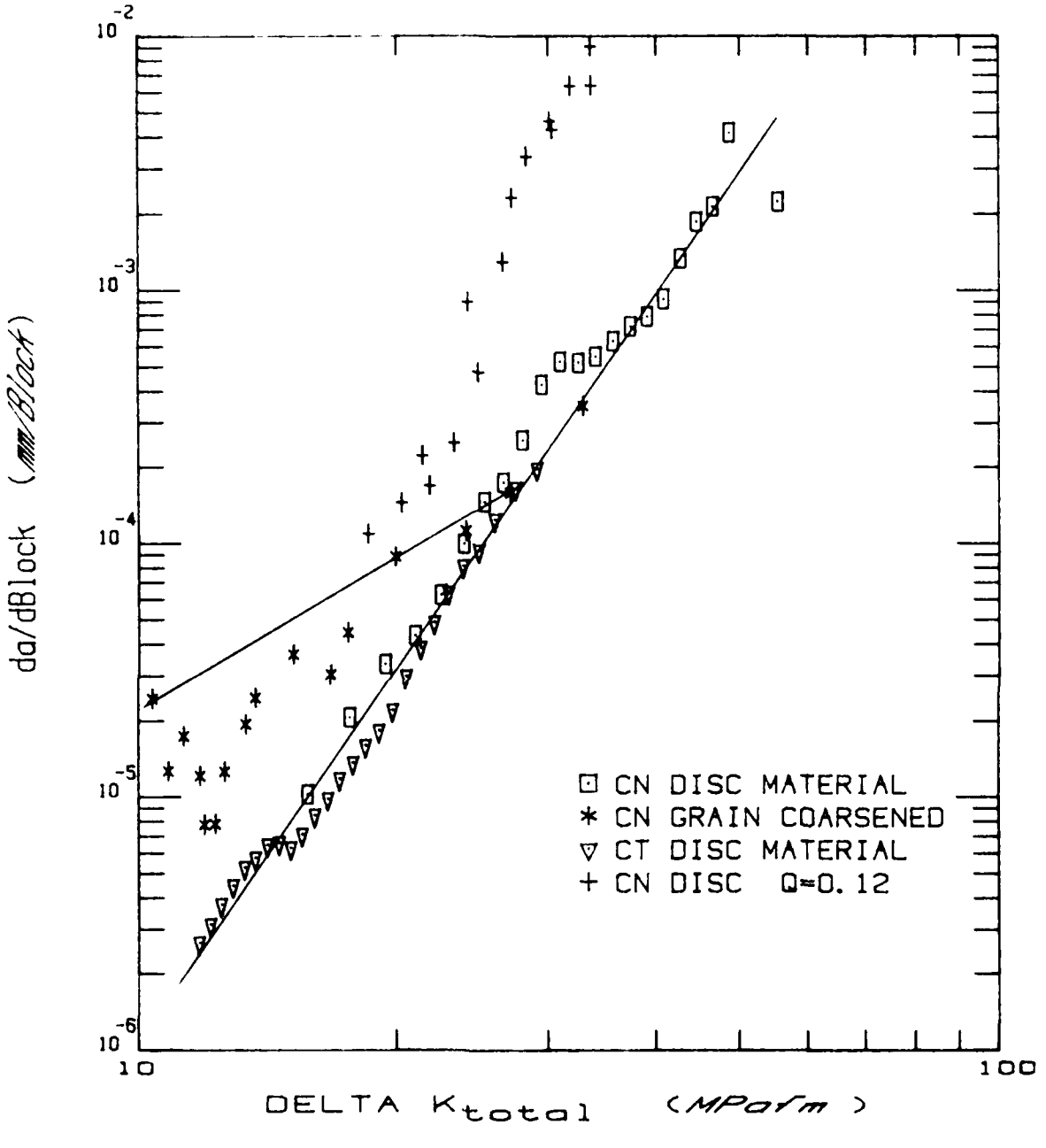

Fig. 36. Summary of FCG rate data for Ti-5331S

below their conventionally determined fatigue threshold value. However, the second test at this amplitude ratio differs significantly from the first in terms of life to a given crack size. In this test the initial crack growth follows very closely that of the major cycles only test, but after approximately 6000 cycles the effect of the minor cycles starts to predominate. This curve suggests that the initial FCG rates are equivalent to those from the application of major cycles only to short cracks, which means that the addition of minor cycles has not enhanced the FCG rate at this stage.

It may be possible to reconcile the difference in FCG lives at an amplitude ratio of 0.22 by assuming that only major cycles produce a short crack effect and that the resulting crack growth rate varies considerably with microstructural features such as grain or colony orientation. Thus where amenable orientations are present, the initial FCG rate due to major load cycles is given by the upper bound of the data from Brown and Hicks(11). This would mean that the length of crack corresponding to ΔK_{onset} is reached very rapidly. Similarly, if the grain orientations are unfavourable the initial FCG rates are comparable to those observed in the major cycle only test for CT specimens, and a longer fatigue life before the onset of minor cycle damage is realised.

To quantify the argument, in the test producing rapid results only 1647 loading blocks were required to grow the crack to a length of 4.4 mm. The predicted ΔK_{onset} condition was reached after an initial growth increment of 0.296 mm. Using the maximum FCG rates for short cracks subjected to major cycle loading defined as the upper bound of the Brown and Hicks data, such a growth increment could be achieved by the application of 777 blocks, leaving 870 blocks for the remaining crack growth in which the contribution from minor cycles above their threshold value would be significant. By comparison in the second test 1606 blocks were required to grow the crack from the predicted minor cycle onset condition to a length of 3.8 mm. Also from the second test the application of 6000 blocks to achieve the predicted onset condition corresponds to an average short crack growth rate within the scatter band for results from major cycle loading.

Clearly the considerable scatter in major cycle FCG rates for short cracks can lead to significant variation in fatigue life where a small increment of crack growth can result in the onset of substantial minor cycle damage. What is not apparent from the limited data available, is whether the results can be explained on the basis of the initial crack growth being entirely due to short crack effects associated solely with major cycle loading, followed by a transition to extensive minor cycle crack growth which is consistent with known long crack behaviour.

SECTION 7

CONCLUSIONS

1. Room temperature fatigue crack growth rates in Ti-6Al-4V and Ti-5331S have been determined using corner notched test pieces consisting of tensile loaded bars containing a single small quarter-circular crack. The loadings employed involve trapezoidal major cycles and sinusoidal minor stress cycles which were applied separately or in combination. The measured crack growth rates have been compared with those generated using compact tension test pieces.

2. In Ti-6Al-4V, a material exhibiting a fine microstructure and limited plasticity-induced crack closure, the crack growth rates occurring in corner notched specimens due solely to the application of major stress cycles were retarded relative to those occurring in compact tension specimens for ranges of stress intensity above 20 MPa$\sqrt{m}$. By contrast, in Ti-5331S, a material possessing a grain size of 0.6 mm and a substantial level of surface roughness-induced crack closure, differences in crack growth rates occurred only when microstructurally short crack effects occurred in the corner notched test pieces.

3. In Ti-6Al-4V subjected to a combination of major and minor stress cycles there is a good agreement between the fatigue crack growth rates obtained from tests carried out on compact tension and corner notched test pieces and those predicted by the linear summation of crack growth associated with the low and high cycle fatigue loadings. In Ti-5331S both accelerations and retardations in growth rates relative to the linear summations have been observed. It is suggested that the accelerations arise from microstructually short crack behaviour, whilst the retardations arise in part from the interaction between the mechanism of cyclic cleavage and striated fatigue crack growth.

4. In exploratory tests using grain coarsened Ti-5331S material, the occurrence of enhanced fatigue crack growth rates for microstructurally short cracks has been observed for a major cycle only loading but not for a minor cycle only loading. Under the conjoint action of major and minor cycles a short crack effect was apparent but the individual contributions from the component stress cycles could not be separated.

REFERENCES

1. POWELL, B.E. and HENDERSON, I. 'The conjoint action of high and low cycle fatigue', AFWAL-TR-83-4119, Air Force Wright Aeronautical Laboratories, Wright-Patterson Air Force Base, Ohio, November 1983.

2. POWELL, B.E. and HENDERSON, I. 'Crack growth in titanium alloys under the conjoint action of high and low cycle fatigue', AFWAL-TR-85-4093, Air Force Wright Aeronautical Laboratories, Wright-Patterson Air Force Base, Ohio, February 1986.

3. HICKS, M.A. and PICKARD, A.C. 'A comparison of theorectical and experimental methods of calibrating the electrical potential drop technique for crack length determination', Int. J. Fracture, 1982, 20, 91-101.

4. ASTM, 'Standard recommended practice for unification of constant amplitude dynamic loads in axial load fatigue testing mechines', ANSI/ASTM Standard E467-67, ASTM Book of Standards, Part 3, 1983, 572-576.

5. ASTM 'Tentative test methods for constant amplitude fatigue crack growth above 10^{-8} m/cycle', ASTM Standard E647-78T, ASTM Book of Standards, Part 3, 1983, 710-730.

6. PICKARD, A.C. 'Stress intensity factors for cracks with circular and elliptic crack fronts, determined by 3-dimensional finite element methods', 2nd Int. Conf. on Numerical Methods in Fracture Mech., Swansea, 1980.

7. PICKARD, A.C. 'The application of 3-dimensional finite element methods to fracture mechanics and fatigue life predictions', EMAS, Warley, UK, 1986.

8. DUNCAN, R.M., GOOSEY, R.E., JEAL, R.H. and POSTANS, P.J. 'Process development and evaluation of gas turbine engine components in IMI 829', 4th Int. Conf. on Titanium, Met. Soc. AIME, New York, 1980, 429-439.

9. PICKARD, A.C., BROWN, C.W. and HICKS, M.A. 'The development of advanced specimen testing and analysis techniques applied to fracture mechanics lifing of gas turbine components', Advances in Life Prediction Methods, New York, 1983, 173-178.

10. BROWN, C.W. and HICKS, M.A. 'Fatigue growth of surface cracks in nickel-based superalloys', Int. J. Fatigue, 1982, 4, 73-81.

11. BROWN, C.W. and HICKS, M.A. 'A study of short fatigue crack growth behaviour in titanium alloy IMI 685', Fatigue Engrg. Mats and Structures, 1983, 6, 67-76.

12. BAXTER, C. Private communication, Rolls-Royce, Aeroengine Division, Derby.

13. WARD-CLOSE, P.E., and BEEVERS, C.J. 'The influence of grain orientation on the mode and rate of fatigue crack growth in α-titanium', Met. Trans., 1980, 11A, 1007-1017.

14. POWELL, B.E. 'The influence of minor cycles on low cycle fatigue crack growth', PhD Thesis (CNAA), Portsmouth Polytechnic, June 1985.

A P P E N D I X

Illustrations of Fatigue Crack Growth in the body of the report have been compiled from the analysis of data obtained from the tests. This appendix contains relevant data derived from analysis of each test.

TEST DATA RECORD

Designated test number	A1
Material specification	Ti-6-4
Area of specimen at gauge length	100 mm^2
Maximum major cycle load applied	50 kN
Minimum major cycle load applied	5 kN
Superimposed minor cycle amplitude	0 kN
Frequency of major load	0.1 Hz
Frequency of minor load	- Hz
Crack length prior to test	0.481 mm
Crack length at end of test	3.715 mm

Elapsed Number of Cycles	Crack Length	Stress Intensity Factor, ΔK	Fatigue Crack Growth Rate
	mm	$MN/m^{3/2}$	nm/cycle
2	.48	-	-
6100	.56	13.93	24.7
9460	.71	15.66	58.0
11100	.85	17.18	106.5
12200	1.00	18.65	146.8
13110	1.15	20.00	179.6
13840	1.30	21.29	222.7
14435	1.44	22.50	271.7
14910	1.59	23.64	309.3
15370	1.73	24.73	321.7
15808	1.88	25.79	367.6
16168	2.03	26.85	421.6
16514	2.18	28.06	476.6
16782	2.32	29.24	565.2
17028	2.47	30.44	688.6
17209	2.61	31.68	798.0
17393	2.76	32.90	887.7
17537	2.91	34.18	1040.5
17676	3.05	35.48	1092.8
17806	3.20	36.82	1287.1
17902	3.34	38.16	1551.9
17995	3.49	39.59	1681.0
18077	3.64	41.01	2015.6
18104	3.71	-	-

TEST DATA RECORD

Designated test number	A2
Material specification	Ti-6-4
Area of specimen at gauge length	100 mm^2
Maximum major cycle load applied	50 kN
Minimum major cycle load applied	5 kN
Superimposed minor cycle amplitude	0 kN
Frequency of major load	0.1 Hz
Frequency of minor load	- Hz
Crack length prior to test	0.515 mm
Crack length at end of test	4.328 mm

Elapsed Number of Cycles	Crack Length mm	Stress Intensity Factor, ΔK $MN/m^{3/2}$	Fatigue Crack Growth Rate nm/cycle
20	.51	-	-
6329	.66	15.06	30.3
10360	.83	16.89	48.7
13140	.99	18.53	82.5
14400	1.16	20.08	157.2
15260	1.32	21.51	189.4
16155	1.49	22.87	212.8
16835	1.66	24.18	273.7
17375	1.83	25.41	331.4
17840	1.99	26.60	386.2
18240	2.16	27.93	427.1
18615	2.32	29.27	478.1
18935	2.49	30.66	597.4
19180	2.66	32.08	746.9
19378	2.82	33.47	885.9
19550	2.99	34.92	973.9
19719	3.16	36.42	1026.3
19878	3.33	38.00	1177.8
20005	3.49	39.59	1426.8
20111	3.66	41.23	1638.4
20207	3.82	42.92	1896.5
20287	3.99	44.71	2530.2
20338	4.15	46.50	3506.6
20382	4.33	-	-

TEST DATA RECORD

Designated test number	A3
Material specification	Ti-6-4
Area of specimen at gauge length	50 mm^2
Maximum major cycle load applied	25 kN
Minimum major cycle load applied	2.5 kN
Superimposed minor cycle amplitude	± 1.35 kN
Frequency of major load	0.1 Hz
Frequency of minor load	150 Hz
Crack length prior to test	0.60 mm
Crack length at end of test	3.46 mm

Elapsed Number of Cycles	Crack Length	Stress Intensity Factor, ΔK_{total}	Fatigue Crack Growth Rate
	mm	$MN/m^{3/2}$	nm/cycle
1	.60	-	-
1605	.74	17.01	87.0
3475	.90	18.80	118.7
4268	1.06	20.43	283.9
4586	1.21	21.95	687.4
4726	1.37	23.40	1672.4
4775	1.53	24.95	3690.1
4812	1.69	26.59	4354.9
4847	1.84	28.22	5438.8
4870	2.00	29.95	7788.3
4888	2.16	31.71	8940.7
4905	2.32	33.49	10010.3
4919	2.47	35.37	11943.7
4932	2.64	37.46	14220.0
4942	2.80	39.58	17029.4
4950	2.95	41.60	20856.4
4957	3.11	44.04	27255.0
4962	3.27	46.51	31197.1
4968	3.46	-	-

TEST DATA RECORD

Designated test number	A4
Material specification	Ti-6-4
Area of specimen at gauge length	50 mm^2
Maximum major cycle load applied	25 kN
Minimum major cycle load applied	2.5 kN
Superimposed minor cycle amplitude	± 1.35 kN
Frequency of major load	0.1 Hz
Frequency of minor load	150 Hz
Crack length prior to test	0.52 mm
Crack length at end of test	2.784 mm

Elapsed Number of Cycles	Crack Length	Stress Intensity Factor, ΔK_{total}	Fatigue Crack Growth Rate
	mm	$MN/m^{3/2}$	nm/cycle
1	.52	-	-
970	.59	15.11	70.3
2820	.72	16.70	84.2
4010	.84	18.18	132.6
4760	.97	19.56	263.3
4990	1.10	20.86	862.6
5057	1.23	22.08	1888.5
5126	1.36	23.27	2274.2
5172	1.49	24.52	3409.9
5202	1.62	25.84	4839.7
5226	1.75	27.23	6239.4
5243	1.87	28.52	7721.1
5258	2.00	29.87	9657.9
5270	2.13	31.37	12506.1
5279	2.26	32.82	14926.1
5288	2.40	34.49	15630.9
5295	2.51	35.81	18111.9
5302	2.66	37.66	22469.6
5307	2.78	-	-

TEST DATA RECORD

Designated test number	A5
Material specification	Ti-6-4
Area of specimen at gauge length	50 mm^2
Maximum major cycle load applied	13.5 kN
Minimum major cycle load applied	1.35 kN
Superimposed minor cycle amplitude	± 1.35 kN
Frequency of major load	0.1 Hz
Frequency of minor load	150 Hz
Crack length prior to test	0.674 mm
Crack length at end of test	2.85 mm

Elapsed Number of Cycles	Crack Length	Stress Intensity Factor, ΔK_{total}	Fatigue Crack Growth Rate
	mm	$MN/m^{3/2}$	nm/cycle
140	.69	-	-
2190	.76	9.72	25.8
7730	.89	10.55	19.3
15700	1.02	11.32	22.0
19600	1.15	12.05	49.2
21280	1.29	12.82	114.9
21870	1.41	13.41	254.3
22255	1.54	14.16	406.9
22515	1.67	14.92	578.0
22705	1.80	15.69	765.8
22855	1.93	16.48	977.7
22975	2.06	17.30	1095.7
23094	2.19	18.12	1159.9
23200	2.33	18.98	1288.1
23296	2.45	19.85	1427.8
23382	2.59	20.78	1628.2
23456	2.71	21.72	1834.6
23524	2.85	-	-

TEST DATA RECORD

Designated test number	A6
Material specification	Ti-6-4
Area of specimen at gauge length	50 mm^2
Maximum major cycle load applied	13 kN
Minimum major cycle load applied	1.3 kN
Superimposed minor cycle amplitude	± 1.3 kN
Frequency of major load	0.1 Hz
Frequency of minor load	150 Hz
Crack length prior to test	0.56 mm
Crack length at end of test	3.039 mm

Elapsed Number of Cycles	Crack Length	Stress Intensity Factor, ΔK_{total}	Fatigue Crack Growth Rate
	mm	$MN/m^{3/2}$	nm/cycle
3	.56	-	-
8275	.66	8.73	11.5
21050	.80	9.63	12.4
30825	.94	10.46	14.4
40450	1.08	11.23	17.9
46375	1.22	11.97	35.7
48325	1.36	12.68	111.4
48875	1.50	13.39	327.5
49179	1.64	14.19	498.8
49439	1.78	14.98	557.6
49675	1.92	15.78	634.1
49880	2.06	16.62	717.3
50070	2.20	17.48	815.5
50220	2.33	18.34	1075.8
50330	2.48	19.28	1406.2
50420	2.62	20.22	1488.9
50515	2.75	21.20	1543.9
50600	2.89	22.24	1828.0
50665	3.03	-	-

TEST DATA RECORD

Designated test number	B1
Material specification	Ti-5331S
Area of specimen at gauge length	100 mm^2
Maximum major cycle load applied	50 kN
Minimum major cycle load applied	5 kN
Superimposed minor cycle amplitude	0 kN
Frequency of major load	0.1 Hz
Frequency of minor load	- Hz
Crack length prior to test	0.535 mm
Crack length at end of test	4.608 mm

Elapsed Number of Cycles	Crack Length	Stress Intensity Factor, ΔK	Fatigue Crack Growth Rate
	mm	$MN/m^{3/2}$	nm/cycle
2	.53	-	-
23860	.72	15.75	10.4
35180	.90	17.65	21.0
40990	1.08	19.37	34.1
45770	1.26	20.98	44.2
49170	1.44	22.48	63.7
51450	1.62	23.90	101.5
52740	1.80	25.26	149.1
53880	1.99	26.56	178.0
54760	2.16	27.97	261.7
55250	2.34	29.44	434.2
55590	2.52	30.93	536.3
55930	2.71	32.49	530.4
56270	2.89	34.01	561.6
56565	3.07	35.61	646.0
56831	3.25	37.27	738.3
57056	3.43	38.98	806.5
57278	3.61	40.73	945.7
57442	3.79	42.61	1361.1
57544	3.97	44.48	1897.5
57631	4.15	46.47	2179.4
57711	4.33	48.56	4247.9
57801	4.87	55.32	2273.0
57830	4.61	-	-

TEST DATA RECORD

Designated test number	B2
Material specification	Ti-5331S
Area of specimen at gauge length	100 mm^2
Maximum major cycle load applied	50 kN
Minimum major cycle load applied	5 kN
Superimposed minor cycle amplitude	0 kN
Frequency of major load	0.1 Hz
Frequency of minor load	- Hz
Crack length prior to test	0.503 mm
Crack length at end of test	4.263 mm

Elapsed Number of Cycles	Crack Length	Stress Intensity Factor, ΔK	Fatigue Crack Growth Rate
	mm	$MN/m^{3/2}$	nm/cycle
9220	.87	-	-
10615	1.01	18.68	120.0
11670	1.17	20.16	97.5
13930	1.33	21.55	73.0
16115	1.49	22.88	100.4
17175	1.66	24.14	167.7
18055	1.82	25.35	223.9
18630	1.98	26.52	328.7
19040	2.14	27.78	475.1
19314	2.31	29.12	655.3
19540	2.47	30.47	737.6
19756	2.63	31.84	817.7
19936	2.79	33.21	872.5
20129	2.96	34.64	862.3
20314	3.12	36.09	845.2
20513	3.28	37.59	872.6
20688	3.45	39.14	936.6
20859	3.61	40.71	959.1
21027	3.77	42.37	1029.8
21177	3.93	44.08	1233.5
21290	4.10	45.83	1631.8
21377	4.26	-	-

TEST DATA RECORD

Designated test number	B3
Material specification	Ti-5331S
Area of specimen at gauge length	50 mm^2
Maximum major cycle load applied	25 kN
Minimum major cycle load applied	2.5 kN
Superimposed minor cycle amplitude	± 1.35 kN
Frequency of major load	0.1 Hz
Frequency of minor load	150 Hz
Crack length prior to test	0.541 mm
Crack length at end of test	3.080 mm

Elapsed Number of Cycles	Crack Length	Stress Intensity Factor, ΔK_{total}	Fatigue Crack Growth Rate
	mm	$MN/m^{3/2}$	nm/cycle
10194	1.00	-	-
10505	1.04	20.25	147.5
11580	1.20	21.83	172.8
12370	1.36	23.31	255.3
12840	1.52	24.87	486.6
13030	1.68	26.52	1319.9
13086	1.85	28.25	3420.6
13127	2.02	30.05	4726.3
13154	2.17	31.77	6470.3
13175	2.33	33.58	9232.4
13190	2.50	35.70	11605.0
13203	2.65	37.58	13243.6
13213	2.81	39.64	17386.8
13222	2.98	42.08	19312.9
13227	3.08	-	-

TEST DATA RECORD

Designated test number	B4
Material specification	Ti-5331S
Area of specimen at gauge length	50 mm^2
Maximum major cycle load applied	24 kN
Minimum major cycle load applied	2.4 kN
Superimposed minor cycle amplitude	± 1.3 kN
Frequency of major load	0.1 Hz
Frequency of minor load	150 Hz
Crack length prior to test	0.515 mm
Crack length at end of test	3.049 mm

Elapsed Number of Cycles	Crack Length	Stress Intensity Factor, ΔK_{total}	Fatigue Crack Growth Rate
	mm	$MN/m^{3/2}$	nm/cycle
3180	.65	-	-
6410	.94	18.51	110.7
8592	1.25	21.42	227.3
9072	1.55	24.16	913.6
9247	1.85	27.16	2359.6
9324	2.14	30.27	4362.0
9383	2.44	33.62	6489.0
9416	2.74	37.27	11664.8
9435	3.05	-	-

TEST DATA RECORD

Designated test number	B5
Material specification	Ti-5331S
Area of specimen at gauge length	50 mm^2
Maximum major cycle load applied	13 kN
Minimum major cycle load applied	1.3 kN
Superimposed minor cycle amplitude	± 1.3 kN
Frequency of major load	0.1 Hz
Frequency of minor load	150 Hz
Crack length prior to test	0.561 mm
Crack length at end of test	3.680 mm

Elapsed Number of Cycles	Crack Length	Stress Intensity Factor, ΔK_{total}	Fatigue Crack Growth Rate
	mm	$MN/m^{3/2}$	nm/cycle
2	.56	-	-
9875	.67	8.81	11.4
24600	.84	9.87	14.5
32775	1.01	10.84	31.8
35100	1.17	11.74	96.5
36275	1.34	12.60	182.2
36924	1.51	13.44	242.4
37704	1.69	14.48	257.8
38224	1.84	15.34	333.6
38654	2.01	16.31	401.1
39054	2.17	17.33	477.9
39344	2.34	18.35	627.0
39584	2.51	19.47	765.3
39784	2.67	20.62	848.8
39976	2.84	21.83	925.1
40140	3.00	23.08	1178.1
40260	3.17	24.47	1875.7
40340	3.38	26.23	2318.3
40404	3.51	27.43	1687.5
40517	3.68	-	-

TEST DATA RECORD

Designated test number	B6
Material specification	Ti-5331S
Area of specimen at gauge length	50 mm^2
Maximum major cycle load applied	13 kN
Minimum major cycle load applied	1.3 kN
Superimposed minor cycle amplitude	± 1.3 kN
Frequency of major load	0.1 Hz
Frequency of minor load	150 Hz
Crack length prior to test	0.624 mm
Crack length at end of test	3.828 mm

Elapsed Number of Cycles	Crack Length	Stress Intensity Factor, ΔK_{total}	Fatigue Crack Growth Rate
	mm	$MN/m^{3/2}$	nm/cycle
1	.62	-	-
6950	.73	9.21	16.5
17150	.90	10.26	21.1
23125	1.07	11.21	35.9
26650	1.25	12.11	47.3
30350	1.42	12.94	65.3
31893	1.59	13.90	99.7
33793	1.76	14.87	119.1
34763	1.93	15.86	201.2
35493	2.10	16.89	284.9
35973	2.28	17.96	485.8
36197	2.44	19.05	728.7
36441	2.62	20.22	690.3
36693	2.79	21.44	734.2
36909	2.96	22.76	1011.9
37033	3.13	24.11	1256.7
37181	3.30	25.56	1315.8
37297	3.48	27.15	1669.7
37385	3.64	28.72	1945.8
37475	3.82	-	-

TEST DATA RECORD

Designated test number	C1
Material specification	Ti-5331S
Area of specimen at gauge length	43 mm^2
Maximum major cycle load applied	20 kN
Minimum major cycle load applied	2 kN
Superimposed minor cycle amplitude	0 kN
Frequency of major load	0.1 Hz
Frequency of minor load	-
Crack length prior to test	0.316 mm
Crack length at end of test	3.816 mm

Elapsed Number of Cycles	Crack Length mm	Stress Intensity Factor, ΔK $MN/m^{3/2}$	Fatigue Crack Growth Rate nm/cycle
0	.31	-	-
1000	.36	10.39	24.9
3002	.39	10.84	12.9
6005	.42	11.30	17.7
7007	.46	11.81	12.3
10007	.47	11.96	7.9
12008	.50	12.31	7.9
16550	.52	12.61	12.9
18715	.58	13.35	19.8
21235	.62	13.71	25.1
25195	.75	15.14	37.1
29156	.91	16.75	31.0
33116	.99	17.53	45.4
37076	1.27	19.92	90.2
41037	1.71	24.04	114.0
43565	2.0[illegible]	[illegible]	161.4
46087	2.52	[illegible]	357.6
48608	3.81	-	-

TEST DATA RECORD

Designated test number	C3
Material specification	Ti-5331S
Area of specimen at gauge length	42 mm^2
Maximum major cycle load applied	19 kN
Minimum major cycle load applied	2.0 kN
Superimposed minor cycle amplitude	1.1 kN
Frequency of major load	0.1 Hz
Frequency of minor load	150 Hz
Crack length prior to test	0.270 mm
Crack length at end of test	3.373 mm

Elapsed Number of Cycles	Crack Length	Stress Intensity Factor, ΔK_{total}	Fatigue Crack Growth Rate
	mm	$MN/m^{3/2}$	nm/cycle
0	.27	-	-
2203	.36	10.53	48.1
4804	.50	12.45	47.3
6804	.58	13.39	23.0
9804	.61	13.84	19.8
11304	.66	14.42	55.0
13304	.81	15.91	49.6
16292	.91	16.96	85.3
18292	1.23	19.83	128.7
19292	1.30	20.36	101.1
20792	1.48	22.15	136.4
21792	1.64	23.66	132.0
22292	1.68	24.08	117.7
24292	1.93	26.63	186.5
24792	2.15	28.94	519.0
24892	2.25	30.01	1665.0
24992	2.48	32.80	729.0
25392	2.61	34.40	288.0
26092	2.80	36.91	400.?
27292	3.37	-	-

TEST DATA RECORD

Designated test number	C4
Material specification	Ti-5331S
Area of specimen at gauge length	41 mm^2
Maximum major cycle load applied	18.2 kN
Minimum major cycle load applied	2.0 kN
Superimposed minor cycle amplitude	± 1.8 kN
Frequency of major load	0.1 Hz
Frequency of minor load	150 Hz
Crack length prior to test	0.352 mm
Crack length at end of test	4.485 mm

Elapsed Number of Cycles	Crack Length	Stress Intensity Factor, ΔK_{total}	Fatigue Crack Growth Rate
	mm	$MN/m^{3/2}$	nm/cycle
0	.35	-	-
1442	2.90	39.11	1895.5
1545	3.28	45.08	7718.0
1647	4.48	-	-

TEST DATA RECORD

Designated test number	C5
Material specification	Ti-5331S
Area of specimen at gauge length	42 mm^2
Maximum major cycle load applied	18.2 kN
Minimum major cycle load applied	2.0 kN
Superimposed minor cycle amplitude	± 1.8 kN
Frequency of major load	0.1 Hz
Frequency of minor load	150 Hz
Crack length prior to test	0.325 mm
Crack length at end of test	3.791 mm

Elapsed Number of Cycles	Crack Length	Stress Intensity Factor, ΔK_{total}	Fatigue Crack Growth Rate
	mm	$MN/m^{3/2}$	nm/cycle
0	.32	-	-
800	.33	10.09	15.9
1700	.35	10.38	21.1
2500	.37	10.63	27.0
3500	.40	11.08	39.6
4000	.43	11.47	53.3
5001	.48	12.16	61.7
5502	.52	12.67	134.4
6005	.61	13.80	900.0
6507	1.42	21.51	1776.1
6608	1.68	24.04	1857.9
6709	1.80	25.18	730.2
7011	1.98	27.04	702.8
7211	2.15	28.90	1938.0
7311	2.56	33.69	2965.5
7411	2.74	36.09	2587.5
7511	3.08	40.84	5220.0
7611	3.79	-	-

LIST OF SYMBOLS AND ABBREVIATIONS

A	product of the general, back and side correction factors
$F(\sigma)$	stress function related to the remote stress distribution
K	stress intensity factor (MPa $\sqrt{m}$)
M_B	back-face correction factor
M_G	general correction factor
M_S	side-face correction factor
P	load (MPa)
Q	ratio of minor cycle amplitude to major cycle amplitude
R	stress ratio
R_{major}	stress ratio for the applied major cycle
R_{minor}	stress ratio for the superimposed minor cycles
V_c	potential difference at the notch
V_c (off)	notch voltage with pulsed current off
V_c (on)	notch voltage with pulsed current on
V_{ref}	potential difference at the reference probes
V_{ref} (off)	reference voltage with pulsed current off
V_{ref} (on)	reference voltage with pulsed current on
W	specimen width (m)
Z	probe spacing at the notch (m)
a	crack length (m)
$\frac{da}{dN}$	crack growth per cycle (mm/cycle)
$\frac{da}{d\ block}$	crack growth per major-minor loading block (mm/cycle)

LIST OF SYMBOLS AND ABBREVIATIONS (CONCLUDED)

n	number of minor cycles per major cycles
ΔK	stress intensity range (MPa $\sqrt{m}$)
ΔK_{major}	stress intensity range associated with the applied major cycle (MPa $\sqrt{m}$)
ΔK_{onset}	value of ΔK_{total} corresponding to the onset of minor cycle crack growth (MPa $\sqrt{m}$)
ΔK_{total}	stress intensity range associated with the total, or overall, stress cycle (MPa $\sqrt{m}$)
CN	corner notched
CT	compact tension
DCPD	direct current potential drop
FCG	fatigue crack growth
HCF	high cycle fatigue
LCF	low cycle fatigue

U.S. GPO 548-054

END
DATE
FILMED
5-88
DTIC